

# Latent Diffusion Model-Enabled Real-Time Semantic Communication Considering Semantic Ambiguities and Channel Noises

Jianhua Pei, *Student Member, IEEE*, Cheng Feng, *Student Member, IEEE*, Ping Wang, *Fellow, IEEE*, Hina Tabassum, *Senior Member, IEEE*, and Dongyuan Shi, *Senior Member, IEEE*

**Abstract**—Semantic communication (SemCom) has emerged as a new paradigm for communication systems, with deep learning (DL) models being one of the key drives to shift from the accuracy of bit/symbol to the semantics and pragmatics of data. Nevertheless, DL-based SemCom systems often face performance bottlenecks due to overfitting, poor generalization, and sensitivity to outliers. Furthermore, the varying-fading gains and noises with uncertain signal-to-noise ratios (SNRs) commonly present in wireless channels usually restrict the accuracy of semantic information transmission. Consequently, to address the aforementioned issues, this paper constructs a SemCom system based on the latent diffusion model, and proposes three improvements compared to existing works: i) To handle potential outliers in the source data, semantic errors obtained by projected gradient descent based on the vulnerabilities of DL models, are utilized to update the parameters and obtain an outlier-robust encoder. ii) A lightweight single-layer latent space transformation adapter completes one-shot learning at transmitter and is placed before the decoder at receiver, enabling adaptation for out-of-distribution data or enhancing human-perceptual quality. iii) An end-to-end consistency distillation (EECD) strategy is used to distill the diffusion models trained in latent space, enabling deterministic single or few-step real-time denoising in various noisy channels while maintaining high semantic quality. Extensive numerical experiments across different datasets demonstrate the superiority of the proposed SemCom system, consistently proving its robustness to outliers, the capability to transmit data with unknown distributions, and the ability to perform real-time channel denoising tasks while preserving high human perceptual quality, outperforming the existing denoising approaches in semantic metrics such as MS-SSIM and LPIPS.

**Index Terms**—Semantic communication, latent diffusion model, GAN inversion, channel denoising, semantic ambiguity.

## I. INTRODUCTION

WITH the booming development of artificial intelligence (AI), augmented and virtual reality [1], 4K/6K streaming [2], and the intelligent sensing devices for smart grids [3] and vehicles [4] within the internet of things (IoT), an efficient and reliable communication system becomes an essential component in the realm of 6-th generation (6G) communications [5]. In information and communication technology, joint source-channel coding (JSCC) [6], [7] is committed to the integrated design of source and channel codes for efficient transmission of data, leveraging Shannon information theory. However, classic JSCC techniques, employing coding methods for engineering applications such as WebP [8], JPEG [9], JPEG2000 [10], and BPG [11], have solely focused on the statistical characteristics of the data being transmitted, disregarding the semantic content they encompass.

Recently, the pursuit of more efficient and intelligent data transmission has given rise to semantic communication (SemCom) systems [12], where the focus is shifted from traditional bit-level accuracy to the conveyance of meaning and intent. The essence of SemCom lies in its capacity to prioritize

the transmission of essential information, thus promising significant improvements in bandwidth utilization and overall communication efficiency [13]. Fortunately, with the rapid advancement of machine learning, deep learning (DL) based SemComs have emerged as an important approach for the implementation of SemCom [14]. Specifically, SemCom built upon neural networks such as variational autoencoder (VAE) [15], residual network (ResNet) [16], convolutional neural network (CNN) [17], long short-term memory (LSTM) network [18], generative adversarial network (GAN) [19], and Transformer [14] have demonstrated effectiveness in extracting the semantic features of source data. This allows for the mapping of source data into a lower-dimensional space for transmission over noisy wireless channels to the receiver, where it can ultimately be decoded back into its original form, whether that be images [20], audio [21], text [14], or multimodal data [22]. Nonetheless, the intrinsic complexity of semantic information, coupled with the unpredictable nature of communication channels, poses new challenges that those SemCom systems are not designed to handle.

Currently, diffusion models (DMs) have taken the forefront in the field of AI-generated content (AIGC) and have achieved remarkable and landmark advancements [23], [24], surpassing other generative models such as VAE [25], GAN [26], and Normalizing Flow (NF) [27]. Consequently, the application of DMs to tackle challenges within SemCom systems is beginning to gain traction [28]. Conditional DM, guided by semantic and free-space information from other users, progressively generate matching data for mixed visual reality applications [29]. Similarly, conditional DMs, guided by invertible neural networks [30], compressed one-hot maps [31], decoded low-quality data [32], and scene graphs [33], have been proposed for image transmission to achieve higher perceptual quality. DMs have also been adapted to rectify errors caused by varying-fading gains and low signal-to-noise ratio (SNR) noises [34]. Wireless channel estimation has also been performed by complex architectures based on DMs [35], [36], whose practicality issues due to high complexity remain to be addressed. Besides serving as decoders for JSCC, DMs can also act as denoisers placed after decoders to enhance data quality [37]. In [38] and [39], prompts, latent embeddings, or noisy data are transmitted over wireless channels to the receiver as starting points or input conditions for DMs, inevitably increasing bandwidth burden. However, the primary bottleneck of DMs lies in their slow data generation speed due to the multi-step prediction process required to improve generation quality, making such time-consuming communica-

tion impractical for real-time SemCom and edge users. Thus, some denoising or encoding methods opt for latent DM (LDM) [40] or acceleration techniques [41], [42] to significantly reduce the computational complexity. Nevertheless, since these enhanced approaches still feature a multi-step process during sampling, they inadequately address the challenges of real-time SemCom.

DMs-based SemCom offers high perceptual quality but also introduces a bottleneck of high latency. Moreover, structural errors or noises and data following unknown distributions can introduce inaccuracies and distortions in the transmitted information when DL-based SemCom systems are deployed. The former, known as semantic errors [43], can arise from exploiting the vulnerabilities of DL models by adversarial attacks that lead to semantic discrepancies. Additionally, when DL-based SemCom system trained by the specific category of data transmits out-of-distribution data [19], [44], the reconstructed data at the receiver may also be semantically ambiguous due to the prevalent issues of poor generalization and overfitting in current AI models. To balance generation quality with speed, LDMs have been chosen as the underlying proposed architecture for the SemCom approach. In summary, while LDMs excel at abstracting and encoding semantic content, the transmission process remains susceptible to semantic ambiguities from semantic errors or out-of-distribution data, i.e., misinterpretations of the meaning or intention behind the transmitted data, and channel noises under different conditions.

To address these issues, this paper presents a comprehensive framework that enhances real-time SemCom by leveraging the capabilities of LDMs while simultaneously considering the effects of semantic ambiguities and channel imperfections. The proposed SemCom model builds upon and enhances the foundational architecture of a pretrained Wasserstein GAN [45] with VAE (VAE-WGAN). The overall contribution of this approach is threefold:

- 1) Semantic errors caused by measurement inaccuracies and cyber attacks can significantly disrupt the normal encoding and decoding of deep JSCC systems. To address this, the vulnerabilities of the pretrained encoder and generator are exploited using convex optimization to determine the most significant undetectable semantic errors. The pretrained encoder is then updated with the obtained semantic errors to refine the neural network parameters, making the encoder robust and resilient to anomalously transmitted data. This parameter update process with data augmentation is self-supervised.
- 2) A rapid domain adaptation strategy is introduced to ensure the reconstructed data is semantically accurate at the receiver when SemCom system transmits data with an unknown distribution. This strategy employs two additional lightweight single-layer neural networks that perform online one-shot or few-shot learning based on adversarial learning strategies. The updated parameters are transmitted to the dynamic neural network deployed at the receiver through the shared knowledge of SemCom system, while the parameters of other networks remain unchanged, thus achieving low-cost out-of-distribution latent space transformation.

- 3) Inspired by channel denoising DMs [40] and consistency distillation [46], the LDM based on ordinary differential equation (ODE) trajectories and variance explosion strategy is trained with known channel state information (CSI) [35], [36]. During the sampling phase, it can denoise the received equalized signals according to different CSIs. Furthermore, the end-to-end consistency distillation (EECD) approach that considers semantic metrics is proposed to distill the trained LDM, ultimately transforming the multi-step denoising process into a deterministic one-step real-time denoising procedure, capable of flexibly addressing varying fading channels and uncertain SNRs.

The efficiency and reliability of the proposed SemCom system in term of perceptual quality and timeliness are validated by rigorous and extensive experiments, providing concrete evidence of its superiority over conventional methods.

The rest of this paper is organized as follows. Section II briefly introduces the proposed wireless SemCom system model and existing challenges. Section III elaborates on the JSCC design of the proposed SemCom system for unknown errors and distributions. The real-time channel denoising implementation is established by EECD in Section IV. Numerical experiments are given in Section V. Section VI concludes the paper. Supporting lemmas are included in the Appendix for reference.

## II. SYSTEM MODEL AND PROBLEM FORMULATION

The proposed SemCom system model depicted in Fig. 1 consists of the encoder  $E_\phi(\cdot)$  with target distribution  $q_\phi(z|x)$ , diffusion model  $\epsilon_\theta(\cdot, \cdot)$  with denoised latent vector's distribution  $p_\theta(z)$ , and decoder  $G_\psi(\cdot)$  with reconstruction target distribution  $q_\psi(x|z)$  by utilizing the synthesized encodings  $z$  from diffusion model. The goal of training this LDM is to learn  $\{\phi, \theta, \psi\}$  by minimizing the overall variational upper bound [47]

$$\begin{aligned}
 \mathcal{L}_{JSCC}(\phi, \theta, \psi) &= \mathbb{E}_{q_\phi(z|x)} [-\log q_\psi(x|z)] + \mathbb{E}_q [\mathcal{D}_{KL}(q_\phi(z|x) \parallel p_\theta(z))] \\
 &= \underbrace{\mathbb{E}_{q_\phi(z|x)} [\log q_\phi(z|x)]}_{\text{transmitter encoding entropy}} + \underbrace{\mathbb{E}_{q_\phi(z|x)} [-\log p_\theta(z)]}_{\text{channel cross entropy}} \\
 &\quad + \underbrace{\mathbb{E}_{q_\phi(z|x)} [-\log q_\psi(x|z)]}_{\text{receiver reconstruction term}}, \tag{1}
 \end{aligned}$$

where  $q_\phi(z|x)$  approximates the true posterior  $q_\psi(z|x)$ . The loss in Eq. (1) has been widely applied and validated in fast data generation [48]. Unlike data generation, the goal of SemCom systems is to make the reconstructed data in receivers shows desired meaning. Consequently, Eq. (1) is divided into three terms: the encoding entropy term at the transmitter, the cross entropy term at the wireless channel, and the reconstruction term at the receiver. However, as stated in Section I, the LDM-enabled SemCom system still faces the following three major challenges:

**1) Semantic Error:** Due to unreasonable measurement, shooting, storage methods, or cyber attacks, the transmitted data may contain some imperceptible errors or noises, which

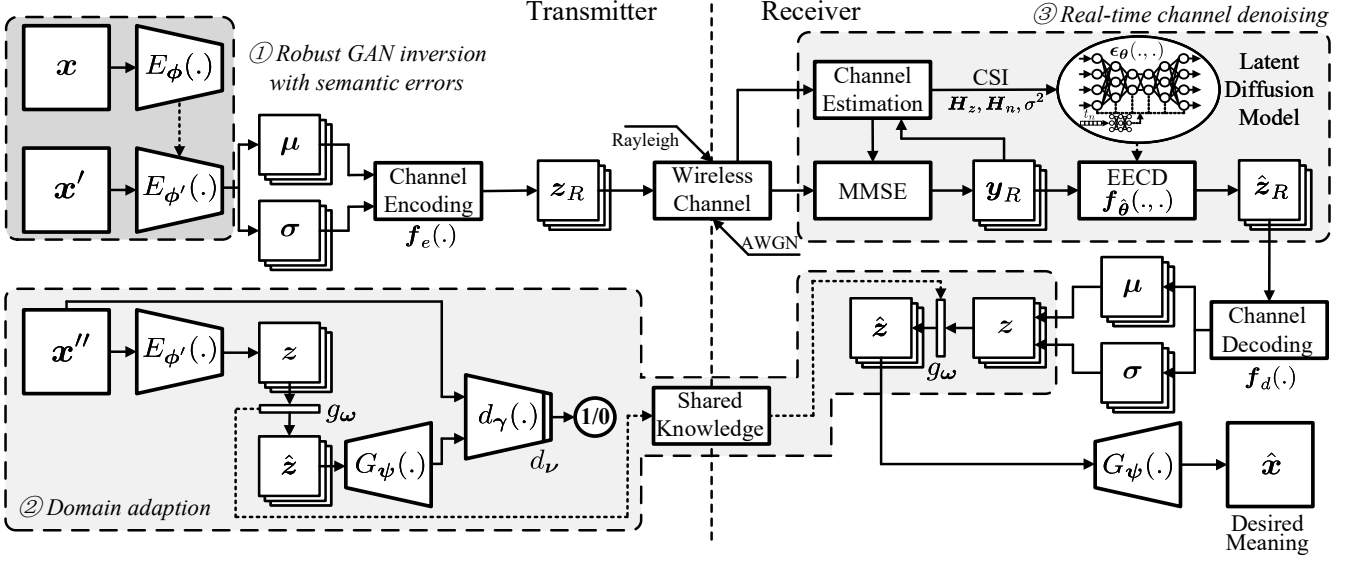


Fig. 1. The proposed semantic communication system model with three addressed deep learning-based communication challenges: ① robust GAN inversion with semantic errors, ② domain adaption with unknown distribution, and ③ real-time wireless channel denoising with end-to-end consistency distillation.

may cause DL-based communication systems to reconstruct data with wrong semantics based on the contaminated data  $x'$  at the receiver. **2) Unknown Distribution:** When a DL-based communication system transmits data  $x''$  with unknown distribution, i.e., the data type is not included in the training dataset, the decoder may generate data with different meaning. A lot of works on transfer learning are dedicated to address the challenge of domain adaptation [19], [44], [49], but strategies for quickly transmit out-of-distribution data still need further exploration. **3) Channel Uncertainties:** The wireless channels are inevitably subjected to varying fading gains and noises with uncertain SNRs. For this reason, the received latent bottleneck is the data  $z'$  with noises and bit errors. Diffusion models can utilize the cross entropy term  $\mathbb{E}_{q_\phi(z|x)}[-\log p_\theta(z)]$  to solve the mapping  $p(z|z')$ , correct bit errors [34], or do joint channel estimation and denoising [35], [36], [40]. Nontheless, these approaches still require uncertain multi-step evaluations to generate clean  $z$ , hindering the real-time implementation of SemCom systems. As a result, the communication objective terms in Eq. (1) are rewritten as:

- Transmitter:  $\mathbb{E}_{q_\phi(z|x'/x'')}[\log q_\phi(z|x'/x'')]$ ,
- Wireless channel:  $\mathbb{E}_{q_\phi(z|x'/x'')}[-\log p_\theta(z|z')]$ ,
- Receiver:  $\mathbb{E}_{q_\phi(z|x'/x'')}[-\log q_\psi(x/x''|z)]$ .

The proposed SemCom system solves the potential problems of DL-based communication system point-to-point. The basic encoder-decoder architecture of the proposed system consists of a variational encoder  $E_\phi(\cdot)$  and generator  $G_\psi(\cdot)$  of WGAN. The fundamental principles and joint training algorithm are detailed in Subsection III-A and Subsection III-B. As illustrated in Fig. 1, the threefold improvements are further clarified as follows:

**1) Robust GAN Inversion:** The imperceptible semantic error that leads to the maximum reconstruction error in DL-based SemCom systems is defined and obtained through adversarial convex optimization. Based on this semantic error, the parameters of the optimized robust encoder are updated from  $\phi$  to  $\phi'$  to encode normal latent space for transmission.

The specific GAN robust inversion method is detailed in Subsection III-C. **2) Domain Adaption:** When transmitting out-of-distribution data, the lightweight single-layer  $g_\omega$  and  $d_\nu$  are exploited for one-shot fast and adversarial domain adaptation learning. The learned parameter  $\omega$  will be simultaneously transmitted to the receiver along with the data for latent space transformation, and the decoder will ultimately output semantically consistent data. The specific implementation can be found in Subsection III-D. **3) Real-time Channel Denoising:** Assume that the CSIs are known, EECD is proposed to distill LDM from multi-step denoising process into one-setp, thereby reducing the computational complexity of online sampling during real-time communication. The detailed wireless channel modeling, training and sampling approaches of the latent channel denoising DM, and one-step real-time channel denoising algorithm are elucidated in Section IV.

### III. DEEP JSCC FOR UNKNOWN ERRORS AND DISTRIBUTIONS

In this section, the selection of the encoder and decoder for the proposed robust and high-quality JSCC is further detailed. In Subsection III-A, WGAN and its higher quality variants are introduced to serve as the decoders for receivers. Subsection III-B firstly presents the joint training algorithm of VAE and WGAN, and Subsection III-C then provides an improved encoder that is robust to measuring errors. The fast and reliable SemCom approach for data of unknown distribution is implemented in Subsection III-D by out-of-distribution latent space exploration.

#### A. Decoder: Wassertein GAN and other variants

In recent years, significant progresses have been made in the generation of ultra-high quality texts, images, and videos in the field of AIGC. The DMs, as an iconic generative model in AIGC, has also received widespread attention. Nevertheless, considering the basic characteristics of the original DMs, SemCom systems built directly based on DMs cannot effectively

improve communication efficiency, i.e., reduce the bandwidth requirements. Therefore, GANs with slightly lower generation quality than DMs are still selected as the decoder for the proposed JSCC. GAN is formulated based on zero-sum game between a discriminator  $D_\gamma(\cdot)$  and a generator  $G_\psi(\cdot)$  with the adversarial training objective

$$\begin{aligned} \min_{\psi} \max_{\gamma} & \mathbb{E}_{\mathbf{x} \sim q(\mathbf{x})} [\log D_\gamma(\mathbf{x})] \\ & + \mathbb{E}_{\mathbf{z} \sim q_\psi(\mathbf{z})} [\log (1 - D_\gamma(G_\psi(\mathbf{z})))], \end{aligned} \quad (2)$$

where  $q_\psi(\mathbf{z})$  is the prior distribution of latent vector  $\mathbf{z}$  and  $q_\psi(\mathbf{z}) = \mathcal{N}(\mathbf{0}, \mathbf{I})$  in GANs. Unfortunately, although GAN can generate higher quality data compared to other generative models such as VAE, it still faces some issues such as training instability and collapse mode. To overcome these challenges, WGAN is established by replacing Kullback-Leibler divergence  $\mathcal{D}_{KL}$  and Jensen-Shannon divergence  $\mathcal{D}_{JS}$  with Wasserstein distance  $\mathcal{D}_W$ . In this way, the optimization objective of WGAN can be decoupled as

$$\begin{aligned} \min_{\psi} \mathbb{E}_{\mathbf{z} \sim q_\psi(\mathbf{z})} [\mathcal{D}_W(\mathbf{x} \parallel G_\psi(\mathbf{z}))] & \Leftrightarrow -\mathbb{E}_{\mathbf{z} \sim q_\psi(\mathbf{z})} [D_\gamma(G_\psi(\mathbf{z}))] \\ \min_{\gamma} -\mathbb{E}_{\mathbf{x} \sim q(\mathbf{x})} [D_\gamma(\mathbf{x})] & + \mathbb{E}_{\mathbf{z} \sim q_\psi(\mathbf{z})} [D_\gamma(G_\psi(\mathbf{z}))]. \end{aligned} \quad (3)$$

Furthermore, the variants of GAN that have been proposed for better perceptual reconstruction can also be utilized as the JSCC decoder. Among them, StyleGAN [50], Diff-GAN trained based on DMs [51], and Diff-Instuct GAN [52] distilled from DMs have achieved impressive generation results, and the latter two models are even comparable to the DMs in some datasets. Consequently, when receivers have higher requirements on decoding data quality, WGAN can be flexibly replaced with these superior variants, as they have the same architecture as the original GANs.

### B. Encoder: GAN Inversion by VAE-WGAN

Compared to VAE, GANs are skilled in generating data with high-resolution. Nonetheless, the task of SemCom is to ensure that the signals received by receivers can accurately convey the meaning, while minimizing the bandwidth of SemCom. For this reason, JSCC requires an encoder to determine the latent bottlenecks of the transmitted data, also known as GAN inversion [53]. Commonly, the solution of GAN inversion is to utilize a neural network-based encoder to find the optimal latent vector  $\mathbf{z}$  given the transmitted data  $\mathbf{x}$ . Ignoring the channel's cross entropy term of the latent space and taking into account the receiver reconstruction term and the transmitter encoding entropy, the variational upper bound can be transformed into

$$\begin{aligned} \mathcal{L}'_{JSCC} &= \mathbb{E}_{q_\phi(\mathbf{z}|\mathbf{x})} [-\log p_\psi(\mathbf{x}|\mathbf{z})] + \mathbb{E}_{q_\phi(\mathbf{z}|\mathbf{x})} [\log q_\phi(\mathbf{z}|\mathbf{x})] \\ &\geq \mathbb{E}_{q_\psi(\mathbf{z})} [-\log p_\psi(\mathbf{x})] + \mathbb{E}_{q(\mathbf{x})} [\mathcal{D}_{KL}(q_\phi(\mathbf{z}|\mathbf{x}) \parallel p_\psi(\mathbf{z}|\mathbf{x}))] \\ &\geq \mathbb{E}_{q_\psi(\mathbf{z})} [-\log p_\psi(\mathbf{x})], \end{aligned} \quad (4)$$

where the proof can be seen in Appendix A. Apparently, the term  $\mathbb{E}_{q_\psi(\mathbf{z})} [-\log p_\psi(\mathbf{x})]$  in Eq. (4) can be replaced with the training objective of the generator  $G_\psi(\cdot)$  of WGAN, and term  $\mathbb{E}_{q(\mathbf{x})} [\mathcal{D}_{KL}(q_\phi(\mathbf{z}|\mathbf{x}) \parallel p_\psi(\mathbf{z}|\mathbf{x}))]$  indicates that the encoding latent vector  $\mathbf{z}$  should be as consistent as possible

with the input latent space of generator  $G_\psi(\cdot)$  under the same transmitted data  $\mathbf{x}$ . Like VAE, the output of encoder can be represented as  $q_\phi(\mathbf{z}|\mathbf{x}) \sim \mathcal{N}(\boldsymbol{\mu}, \boldsymbol{\sigma}^2)$ , and  $\mathbf{z}$  is reparameterized as  $\mathbf{z} = \boldsymbol{\mu} + \boldsymbol{\sigma} \odot \boldsymbol{\epsilon}$ , where  $\boldsymbol{\epsilon} \sim \mathcal{N}(\mathbf{0}, \mathbf{I})$  and  $\odot$  denotes the element-wise product. Consequently, by combining the decoupled optimization objectives of WGAN and Eq. (4), the optimization objectives for the encoder, generator, and discriminator of JSCC are

- Encoder  $E_\phi(\cdot)$ :  $\mathbb{E}_q [\alpha_\phi \mathcal{D}_{KL}(E_\phi(\mathbf{x}) \sim \mathcal{N}(\boldsymbol{\mu}, \boldsymbol{\sigma}^2) \parallel \mathbf{z} \sim \mathcal{N}(\mathbf{0}, \mathbf{I})) + (1 - \alpha_\phi) \mathcal{D}_{KL}(G_\psi(E_\phi(\mathbf{x})) \parallel \mathbf{x})]$ ,
- Generator  $G_\psi(\cdot)$ :  $\mathbb{E}_q [\alpha_\phi \mathcal{D}_{KL}(G_\psi(E_\phi(\mathbf{x})) \parallel \mathbf{x}) + (1 - \alpha_\psi) (-D_\gamma(G_\psi(\mathbf{z})) - D_\gamma(G_\psi(E_\phi(\mathbf{x}))))]$ ,
- Discriminator  $D_\gamma(\cdot)$ :  $\mathbb{E}_q [-D_\gamma(\mathbf{x}) + D_\gamma(G_\psi(\mathbf{z})) + D_\gamma(G_\psi(E_\phi(\mathbf{x})))]$ ,

where  $\alpha_\phi$  and  $\alpha_\psi$  are the loss balance hyperparameters. The training process of deep CNN based VAE-WGAN with gradient penalty [54] is illustrated in Appendix B.

### C. Robust Encoder

As discussed in Section II, VAE-WGAN based SemCom systems suffer from inevitable vulnerabilities, i.e., the covert errors of sampled or measured data  $\mathbf{x}$  or latent vectors  $\mathbf{z}$  transmitted in wireless channels can lead to the receiver's decoding outputs  $\hat{\mathbf{x}}$  that are inconsistent with the original data  $\mathbf{x}$ , ultimately resulting in semantic errors. The adversarial attack methods explores the vulnerabilities of neural networks utilized for classification and regression tasks, with the goal of determining a sufficiently small and unnoticed measurement error  $\boldsymbol{\delta}$  to mislead the classification or regression results. The unified optimization objective of adversarial attacks is given by

$$\begin{aligned} \min_{\boldsymbol{\delta}} & \mathbf{d}(\mathbf{x}, \mathbf{x} + \boldsymbol{\delta}) \\ \text{s.t.: } & \mathbf{f}(\mathbf{x} + \boldsymbol{\delta}) = \text{target}, \quad \mathbf{L} \leq \mathbf{x} + \boldsymbol{\delta} \leq \mathbf{U}, \end{aligned} \quad (5)$$

where  $\mathbf{d}(\cdot, \cdot)$  is the distance function,  $\mathbf{f}(\cdot)$  is the attacked neural network, target denotes the output of the DL model,  $\mathbf{L}$  and  $\mathbf{U}$  represent the physical lower and upper bounds of input data  $\mathbf{x}$ , respectively. Specifically, in classification tasks, target is the class that is inconsistent with original category of  $\mathbf{x}$ , e.g., the hackers can exploit objective (5) to make their cyber attacks undetectable by network  $\mathbf{f}(\cdot)$ . In regression tasks, target represents the output data that is not the same as the original regression results, e.g., when transmitting a digital image in SemCom systems, the receiver's decoder may reconstruct another type of digital image, resulting in semantic ambiguity and seriously reducing the reliability of security of SemCom systems.

In order to address the challenges of semantic errors, SemCom systems should have a robust and enhanced encoder that can handle those outliers. The objectives for the sufficiently small semantic error that leads to the maximum encoding error or reconstruction error are given by

$$\begin{aligned} \max_{\boldsymbol{\delta}} & \mathbf{d}(E_\phi(\mathbf{x}), E_\phi(\mathbf{x} + \boldsymbol{\delta})) \\ \text{s.t.: } & E_\phi(\mathbf{x} + \boldsymbol{\delta}) \sim \mathcal{N}(\mathbf{0}, \mathbf{I}), \|\boldsymbol{\delta}\|_p \leq \varepsilon, \mathbf{L} \leq \mathbf{x} + \boldsymbol{\delta} \leq \mathbf{U} \end{aligned} \quad (6)$$

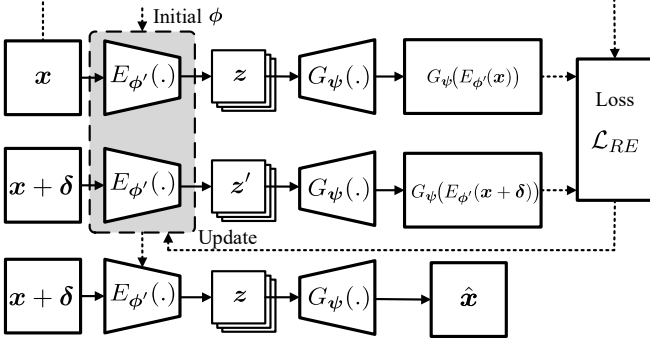


Fig. 2. Self-supervised robust encoder optimization with semantic error  $\delta$ .

and

$$\begin{aligned} \max_{\delta} \quad & \mathbf{d}(G_\psi(E_\phi(x)), G_\psi(E_\phi(x + \delta))) \\ \text{s.t.:} \quad & E_\phi(x + \delta) \sim \mathcal{N}(\mathbf{0}, \mathbf{I}), \|\delta\|_p \leq \varepsilon, \mathbf{L} \leq x + \delta \leq \mathbf{U}, \end{aligned} \quad (7)$$

respectively, where  $\|\cdot\|_p$  denotes the p-norm. In this way, objective (6) utilizes the vulnerability of the encoder  $E_\phi(\cdot)$ , while objective (7) simultaneously utilizes the vulnerabilities of both the encoder  $E_\phi(\cdot)$  and generator  $G_\psi(\cdot)$ . When solving Eq. (7), its objective can be transformed into a standard convex optimization problem

$$\begin{aligned} \min_{\delta} \quad & \underbrace{\lambda \|\delta\|_p - \mathbf{d}(G_\psi(E_\phi(x)), G_\psi(E_\phi(x + \delta)))}_{e(\delta)} \\ \text{s.t.:} \quad & E_\phi(x + \delta) \sim \mathcal{N}(\mathbf{0}, \mathbf{I}), \mathbf{L} \leq x + \delta \leq \mathbf{U}, \end{aligned} \quad (8)$$

where  $\lambda$  is the penalty coefficient. The constrained convex optimization problem can be solved by using the projected gradient descent (PGD) [55] iterative optimization method to obtain semantic error  $\delta$ . Consequently, the semantic error at the  $i$ -th iteration  $\delta^i$  is denoted by

$$\delta^i = P_C(\delta^{i-1} - \eta \nabla_{\delta} e(\delta^{i-1})) = P_C(\varsigma^i), \quad (9)$$

where  $P_C(\varsigma^i)$  represents the projection of  $e(\delta)$  on the set of constraints  $C$ , i.e.,  $\delta^i = P_C(\varsigma^i) := \arg \min_{\delta \in C} \frac{1}{2} \|\delta - \varsigma^i\|_2^2$ . Let  $z'$  be the erroneous latent vector encoded from data containing semantic errors  $x' = x + \delta$ , the robust variational upper bound for semantic errors is defined as

$$\begin{aligned} \mathbb{E}_q[-\log p_\psi(x)] &= \mathbb{E}_q[-\log p_\psi(x, x + \delta) d(x + \delta)] \\ &\leq \mathbb{E}_{q(z)}[-\log p_\psi(x|z)] + \mathbb{E}_{q(z)}[-\log p_\psi(z)] \\ &+ \mathbb{E}_{q(z')}[-\log p_\psi(z')] + \frac{\beta}{2} \mathbb{E}_{q(z, z')} d(z, z') \\ &- \mathbb{E}_{q(z, z')}[-\log q(z, z')], \end{aligned} \quad (10)$$

where  $\beta$  denotes the nonnegative coupling parameter. Evidently, the first and second term of Eq. (10) have been addressed in VAE-WGAN based JS-CC, and the third term has also been optimized by sloving the semantic errors  $\delta$ . For this reason, the training objective of robust encoder is

$$\min_{\phi'} \frac{\beta}{2} \mathbb{E}_{q(z, z')} d(z, z') + \mathbb{E}_{q(z, z')} [\log q(z, z')]. \quad (11)$$

In [56], the objective (11) is equivalent to minimizing the Wasserstein distance between  $z$  and the incorrect  $z'$ . Nevertheless, the ultimate goal of SemCom is to accurately reconstruct the transmitted data. Therefore, as the parameter  $\psi$  is fixed, the

**Algorithm 1:** Training algorithm of robust GAN inversion  $E_{\phi'}(\cdot)$

---

**Input:** Dataset  $q(x)$ , learning rate  $\eta_1$  and  $\eta_2$ , original encoder  $E_\phi(\cdot)$ , generator  $G_\psi(\cdot)$ ,  
**Output:** The updated robust encoder  $E_{\phi'}(\cdot)$

- 1 **Initialize**  $\phi' \leftarrow \phi$ ;
- 2 **repeat**
- 3     Sample  $x \sim q(x)$ ;
- 4     Initialize  $\delta^0 \leftarrow \mathbf{0}$  and  $i \leftarrow 1$ ;
- 5     **repeat**
- 6         Compute  $\delta^i \leftarrow P_C(\delta^{i-1} - \eta_1 \nabla_{\delta} e(\delta^{i-1}))$ ;
- 7         Update  $i \leftarrow i + 1$ ;
- 8     **until** *Converged*;
- 9     Determine  $\delta$  by  $\delta \leftarrow \delta^k$ ;
- 10     Update  $\phi'$  by
- 11          $\phi' \leftarrow \phi' - \eta_2 \nabla_{\phi'} [\mathbb{E}_q (\mathbf{d}(x, G_\psi(E_{\phi'}(x))) + \mathbf{d}(G_\psi(E_{\phi'}(x)), G_\psi(E_{\phi'}(x + \delta))))]$ ;
- 11 **until** *Converged*;
- 12 **Return** Robust GAN inversion  $E_{\phi'}(\cdot)$

---

optimal robust encoder parameter  $\phi'$  considering both encoder and decoder vulnerabilities is

$$\phi' = \arg \min_{\phi'} \mathcal{L}_{RE} = \arg \min_{\phi'} \mathbb{E}_q [\mathbf{d}(x, G_\psi(E_{\phi'}(x))) + \mathbf{d}(G_\psi(E_{\phi'}(x)), G_\psi(E_{\phi'}(x + \delta)))] \quad (12)$$

In summary, the self-supervised training process of robust encoder with prior VAE-WGAN is depicted in Fig. 2 and illustrated in Algorithm 1.

#### D. Out-of-Distribution Latent Space

Currently, one of the biggest application bottlenecks of DL-based SemCom is their generalization performance, which means that these machine learning models will significantly degrade their performances when facing data types that are not included in the training dataset. Specifically, the data type within the training dataset is referred to as *in domain*, while data with an unknown distribution for those models can be referred to as *out-of-domain*. For the proposed VAE-WGAN architecture based SemCom, when the transmitter wants to send an out-of-distribution data, robust encoder  $E_{\phi'}$  may encode an abnormal latent vector, and the decoder at the receiver will reconstruct data that is semantically different from the transmitted data. For this reason, when facing these unknown distributions, JS-CC should improve its generalization abilities and be able to quickly adapt to search for the optimal out-of-distribution latent space.

In addition to the learning-based approaches, another approach of GAN inversion can be established by convex optimization. Given the generator  $G_\psi(\cdot)$  pre-trained in a specific domain and a data  $x''$  following an unknown distribution, the optimization objective [57] for the optimal latent vector corresponding to  $G_\psi(\cdot)$  is denoted by

$$\begin{aligned} \min_{\hat{z}} \quad & \mathbf{d}(x'', G_\psi(\hat{z})) + \rho(\hat{z}) \\ \text{s.t.:} \quad & \hat{z} \sim \mathcal{N}(\mathbf{0}, \mathbf{I}), \end{aligned} \quad (13)$$

where  $\rho(\cdot)$  is a penalty term aimed at making  $\hat{z}$  follow the prior distribution of generator  $G_\psi(\cdot)$ , i.e.,  $\hat{z} \sim q_\psi(z)$ . Similar to the

**Algorithm 2:** Online training algorithm of out-of-distribution adaptor  $g_\omega(\cdot)$

**Input:** Data following unknown distribution  $q(\mathbf{x}'')$ , learning rate  $\eta$ , gradient penalty coefficient  $\lambda$ , robust encoder  $E_{\phi'}(\cdot)$ , generator  $G_\psi(\cdot)$ , discriminator  $D_\gamma(\cdot)$  and the parameters of last layer (L-th layer) is denoted by  $\gamma^L$   
**Output:** The online-updated adaptor  $g_\omega(\cdot)$

- 1 **Initialize**  $\omega \leftarrow \mathbf{1}$  and  $\nu \leftarrow \gamma^L$ ;
- 2 **repeat**
- 3     Sample  $\mathbf{x}'' \sim q(\mathbf{x}'')$ ,  $\mathbf{z} \sim q_\psi(\mathbf{z})$ , and  $\epsilon \sim U[0, 1]$ ;
- 4     Compute  $\hat{\mathbf{x}} \leftarrow \epsilon \mathbf{x}'' + (1 - \epsilon) G_\psi(g_\omega(\mathbf{z}))$ ;
- 5     Update  $\nu \leftarrow \nu - \eta \nabla_\nu \left[ \mathbb{E}_q \left( -d_\nu(d_\gamma(\mathbf{x}'')) + d_\nu(G_\psi(g_\omega(\mathbf{z}))) + \lambda (\|\nabla_{\hat{\mathbf{x}}} d_\nu(d_\gamma(\hat{\mathbf{x}}))\|_2 - 1)^2 \right) \right]$ ;
- 6     Update  $\omega \leftarrow \omega - \eta \nabla_\omega \left[ \mathbb{E}_q \left( -d_\nu(d_\gamma(G_\psi(g_\omega(\mathbf{z})))) \right) \right]$ ;
- 7 **until** Converged;
- 8 **Return** the parameters  $\omega$  of adaptor  $g_\omega(\cdot)$

convex optimization problem of semantic error  $\delta$ , objective (13) can also be solved through PGD without using an additional encoder. Nonetheless, this convex optimization problem can take tens to hundreds of iterations each time, so it cannot guarantee the timeliness of SemCom. To address this issue, a learning-based adaptor constructed by a lightweight single-layer neural network is utilized for out-of-distribution latent space determination. Considering the characteristics of VAE-WGAN, as shown in Fig. 3, the adapter  $g_\omega(\cdot)$  parameterized by  $\omega$  is placed between the robust encoder and generator. Subsequently, when the transmitted data follows an unknown distribution, adaptor  $g_\omega(\cdot)$  can perform one-shot learning to transform the latent vector  $\mathbf{z}$  encoded by  $E_{\phi'}(\cdot)$  into

$$\hat{\mathbf{z}} = g_\omega(\mathbf{z}) = \omega^\top \mathbf{z} + \mathbf{b}, \quad (14)$$

where  $\mathbf{b}$  denotes the bias of adaptor  $g_\omega(\cdot)$ . In order to improve the data quality of reconstruction, inspired by the adversarial training startegy of WGAN, this paper considers another adaptor  $d_\nu(\cdot)$  composed of a lightweight fully connected (FC) layer for adversarial training with  $g_\omega(\cdot)$ . As illustrated in Fig. 3, during online training, the FC layer of discriminator  $D_\gamma(\cdot)$  is replaced by  $d_\nu(\cdot)$ , and the original discriminator after removing the FC layer is denoted by  $d_\gamma(\cdot)$ . In this way, the online training process of  $g_\omega(\cdot)$  is similar to WGAN's training approach as illustrated in Algorithm 2.

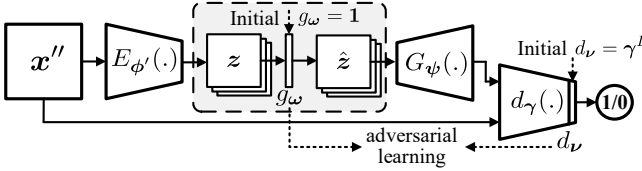


Fig. 3. Out-of-domain latent space determination using lightweight single-layer network and adversarial training method.

In summary, when the SemCom system transmits data *in domain*, the parameters  $\omega$  of  $g_\omega(\cdot)$  is equal to  $\mathbf{1}$ , while transmitting *out-of-domain* data, online learning Algorithm 2 will be activated. Due to the limited amount of training data and the fact that the given initial values of  $\hat{\mathbf{z}}$  and  $\omega$  are close to the optimal values, this online-updated process is very fast. When the online-learning is completed, in order to not change

the weights  $\phi'$ ,  $\psi$ , and  $\theta$  of robust encoder, generator, and LDM utilized for channel denoising by additional transfer learning, the adaptor is deployed at the receiver and defined as a dynamic lightweight nerual network. In other words, the parameter of the implemented adaptor  $g_\omega(\cdot)$  can be dynamically changed through shared knowledge of SemCom system as shown in Fig. 1. Ultimately, the semantically consistent out-of-distribution data is reconstructed according to  $\hat{\mathbf{z}} = g_\omega(\mathbf{z})$ .

#### IV. LATENT CHANNEL DENOISING DIFFUSION MODEL

In this section, the wireless channel equalization under different conditions is firstly established in Subsection IV-A. The training objectives of original LDMs based on the received signals and its one-step real-time implementation are introduced in Subsection IV-B and IV-C.

##### A. Wireless Channel Equalization

Through the joint encodeing of JSCC composed of robust encoder  $E_{\phi'}(\cdot)$  and generator  $G_\psi(\cdot)$ , the robust encoder encodes the original data  $\mathbf{x}$  into a low-dimensional latent bottleneck  $\mathbf{z}$ . Assume that the latent vector  $\mathbf{z}$  needs to reach the receiver through  $k$  wireless channels, the transmitted complex latent signal is denoted by  $\mathbf{z}_c \in \mathbb{C}^k$ . At time  $t$ , the complex signal  $y_{c,i}$  received by the receiver on the  $i$ -th wireless channel can be represented as

$$y_{c,i} = h_{c,i} z_{c,i} + n_{c,i}, \quad (15)$$

where  $\mathbf{h}_c(t) = \sum_{i=1}^k \alpha_i e^{-j2\pi f \tau_i(t)}$ ,  $\alpha_i$  is the signal amplitude of  $i$ -th path,  $f$  is the carrier frequency,  $\tau_i(t)$  denotes the phase shift,  $\mathbf{n}_c \sim \mathcal{CN}(\mathbf{0}, \sigma^2 \mathbf{I})$  represents the complex Gaussian noises. Considering the effects of multipath fading and scattering,  $h_{c,i}$  are independent and identically distributed (i.i.d.) Rician fading gains, which can be denoted by

$$h_{c,i} = \sqrt{\frac{K}{K+1}} + \sqrt{\frac{1}{K+1}} h_{\text{Rayleigh},i}, \quad (16)$$

where  $h_{\text{Rayleigh},i}$  are i.i.d. Rayleigh fading gains and  $K$  is the ratio of direct radio waves' power and non-direct radio waves' power. When  $K = \infty$ , the wireless channels become additive white Gaussian noise (AWGN) channels, and the channels become Rayleigh channels when  $K = 0$ . Optionally, minimum mean square error (MMSE) is utilized as a method for received signals equalization to avoid errors and improve efficiency. Consequently, the addressed signals can be denoted by

$$\begin{aligned} \mathbf{y}_{eq} &= (\mathbf{h}_c^H \mathbf{h}_c + \sigma^2 \mathbf{I})^{-1} \mathbf{h}_c^H (\mathbf{h}_c \mathbf{z}_c + \mathbf{n}_c) \\ &= (\mathbf{h}_c^H \mathbf{h}_c + \sigma^2 \mathbf{I})^{-1} \mathbf{h}_c^H \mathbf{h}_c \mathbf{z}_c + (\mathbf{h}_c^H \mathbf{h}_c + \sigma^2 \mathbf{I})^{-1} \mathbf{h}_c^H \mathbf{n}_c. \end{aligned} \quad (17)$$

For simplicity, the transmitted complex signals  $\mathbf{z}_c$  can also be rewritten as  $\mathbf{z}_R \in \mathbb{R}^{2k}$  in real-valued symbols, the equalization can be defined as  $\mathbf{y}_R \in \mathbb{R}^{2k}$ . In this way, the 1-st to  $k$ -th signals of  $\mathbf{y}_R$  are

$$y_{R,i} = \frac{|h_{c,i}|^2}{|h_{c,i}|^2 + \sigma^2} z_{R,i} + \frac{\text{Re}(h_{c,i}^H)}{|h_{c,i}|^2 + \sigma^2} \sigma \epsilon, \quad (18)$$

where  $\epsilon \sim \mathcal{N}(0, 1)$ . And the  $k + 1$ -th to  $2k$ -th signals can be defined as

$$y_{R,i} = \frac{|h_{c,i}|^2}{|h_{c,i}|^2 + \sigma^2} z_{R,i} + \frac{\text{Im}(h_{c,i}^H)}{|h_{c,i}|^2 + \sigma^2} \sigma \epsilon. \quad (19)$$

To this end, the diagonal matrices  $\mathbf{H}_z$  and  $\mathbf{H}_n$  can be defined as

$$\mathbf{H}_z = \text{diag} \left( \frac{|h_{c,1}|^2}{|h_{c,1}|^2 + \sigma^2}, \dots, \frac{|h_{c,k}|^2}{|h_{c,k}|^2 + \sigma^2}, \frac{|h_{c,1}|^2}{|h_{c,1}|^2 + \sigma^2}, \dots, \frac{|h_{c,k}|^2}{|h_{c,k}|^2 + \sigma^2} \right), \quad (20)$$

$$\mathbf{H}_n = \text{diag} \left( \frac{\text{Re}(h_{c,1}^H)}{|h_{c,1}|^2 + \sigma^2}, \dots, \frac{\text{Re}(h_{c,k}^H)}{|h_{c,k}|^2 + \sigma^2}, \frac{\text{Im}(h_{c,1}^H)}{|h_{c,1}|^2 + \sigma^2}, \dots, \frac{\text{Im}(h_{c,k}^H)}{|h_{c,k}|^2 + \sigma^2} \right). \quad (21)$$

As a consequence, the conditional distribution of  $\mathbf{y}_R$  under the estimated different wireless CSI, i.e.,  $\mathbf{h}_c$  and SNRs, is

$$q_{\text{MMSE}}(\mathbf{y}_R | \mathbf{z}_R, \mathbf{H}_z, \mathbf{H}_n) = \mathcal{N}(\mathbf{y}_R; \mathbf{H}_z \mathbf{z}_R, \mathbf{H}_n^2 \sigma^2 \mathbf{I}). \quad (22)$$

### B. Latent Diffusion Model

The denoising task of receiver is to find the original transmitted signals  $\mathbf{z}_R$  from transmitter given  $\mathbf{y}_R$  and CSI. Accordingly, let  $\mathbf{z}_0 = \mathbf{H}_z \mathbf{z}_R$ , the cross-entropy term in SemCom system model can be transformed from  $\mathbb{E}_{q_{\phi}(\mathbf{z}|\mathbf{x})}[-\log p_{\theta}(\mathbf{z}|\mathbf{x}')]$  to  $\mathbb{E}_q[-\log p_{\theta}(\mathbf{z}_0 | \mathbf{y}_R, \mathbf{H}_z, \mathbf{H}_n)]$ . LDM is selected for wireless channel denoising as it has powerful capabilities to generate realistic data and much lower computational complexity than the original DMs. Let  $\{\mathbf{z}_t\}_{t=0}^{t=T}$  be the noisy latent bottlenecks containing noises of different SNRs in the continuous time domain  $t \in [0, T]$ , where  $\mathbf{z}_0$  is the starting latent vector. LDM defines a forward process through a unified stochastic differential equation (SDE)

$$d\mathbf{z} = \mathbf{u}(\mathbf{z}, t) dt + \mathbf{g}(t) d\mathbf{w}_t, \quad (23)$$

where  $\mathbf{u}(\mathbf{z}, t)$  and  $\mathbf{g}(t)$  are the drift and diffusion coefficients, and  $\mathbf{w}_t$  is a standard Brownian motion. By considering the reverse process of SDE, the marginal distribution  $p(\mathbf{z}_t)$  follows the solution trajectory of the probability flow-ODE (PF-ODE)

$$d\mathbf{z} = \left[ \mathbf{u}(\mathbf{z}, t) - \frac{1}{2} \mathbf{g}^2(t) \nabla_{\mathbf{z}} \log p(\mathbf{z}_t) \right] dt, \quad (24)$$

where  $\nabla_{\mathbf{z}} \log p(\mathbf{z}_t)$  denotes the score function. Accordingly, similar to EDM [58], considering the conditional distribution in Eq. (22), this paper sets  $\mathbf{u}(\mathbf{z}, t) = 0$ ,  $\mathbf{g}(t) = \sqrt{2t} \mathbf{H}_n$ , and  $\sigma(t) = \mathbf{H}_n t$ , where  $t \in [0, T]$ . When solving the reverse sampling trajectory,  $t$  requires a discrete schedule  $\{t_n\}_{n=0}^{n=N}$ . Concretely, when  $n = 0$ ,  $t_0 = 0$ , and when  $n \geq 1$ ,  $t_n = \left( t_1^{1/\rho} + \frac{n-1}{N-1} \left( t_N^{1/\rho} - t_1^{1/\rho} \right) \right)^{\rho}$ , where  $\rho > 0$ . Moreover, unlike denoising diffusion probabilistic model (DDPM) [23], the utilized diffusion model adopts variance explosion (VE) strategy, and its associated forward process  $\{\mathbf{z}_t\}_{t=0}^{t=T}$  can be written as

$$q(\mathbf{z}_t | \mathbf{z}_0) = \mathcal{N}(\mathbf{z}_t; \mathbf{z}_0, t^2 \mathbf{H}_n^2 \mathbf{I}). \quad (25)$$

In the reverse process, the denoising U-Net is usually utilized to predict  $s_{\theta}(\mathbf{z}, t)$  to approximate the score function  $\nabla_{\mathbf{z}} \log p(\mathbf{z}_t)$ . Noise prediction model  $\epsilon_{\theta}(\mathbf{z}_t, t)$  are one of the most popular implementations of diffusion models, and  $s_{\theta}(\mathbf{z}, t) = -\frac{\epsilon_{\theta}(\mathbf{z}_t, t)}{\mathbf{H}_n t}$ . As a consequence, the training objective of LDM is to minimize the loss

$$\begin{aligned} \mathcal{L}_{\text{LDM}} &= \mathbb{E}_q \left[ \|s_{\theta}(\mathbf{z}, t) - \nabla_{\mathbf{z}} \log p(\mathbf{z}_t)\|_2^2 \right] \\ &= \mathbb{E}_{\mathbf{z}_R \sim q_{\phi'}(\mathbf{z}_R | \mathbf{x}), \epsilon_1 \sim \mathcal{N}(\mathbf{0}, \mathbf{I}), n \sim \mathcal{U}[1, N]} \\ &\quad \left[ \left\| \frac{\epsilon_{\theta}(\mathbf{H}_z \mathbf{z}_R + \mathbf{H}_n t_n \epsilon_1, t_n)}{\mathbf{H}_n t_n} - \frac{\epsilon}{\mathbf{H}_n t_n} \right\|_2^2 \right] \quad (26) \\ &\Leftrightarrow \mathbb{E}_q \left[ \|\epsilon_{\theta}(\mathbf{z}_t, t) - \epsilon\|_2^2 \right]. \end{aligned}$$

The PF-ODE defined in Eq. (24) can be rewritten as

$$\frac{d\mathbf{z}_t}{dt} = \epsilon_{\theta}(\mathbf{z}_t, t). \quad (27)$$

Similar to the channel denoising DM in [40], the variational evidence upper bound for wireless channel denoising tasks should consider different CSI conditions and practical DMs implementations, which is given by

$$\begin{aligned} \mathcal{L}'_{\text{LDM}} &= \mathbb{E}_q \left[ -\log p_{\theta}(\mathbf{z}_0 | \mathbf{y}_R, \mathbf{H}_{z/n}) \right] \\ &\leq \mathbb{E}_q \left[ -\log \left( \frac{p_{\theta}(\mathbf{z}_{t_0:t_m}, \mathbf{y}_R | \mathbf{H}_{z/n})}{q(\mathbf{z}_{t_1:t_m}, \mathbf{y}_R | \mathbf{z}_0, \mathbf{H}_{z/n})} \right) \right] \\ &= \mathbb{E}_q \left[ \underbrace{D_{\text{KL}}(q_{\text{MMSE}}(\mathbf{y}_R | \mathbf{z}_0, \mathbf{H}_{z/n}) \| p(\mathbf{y}_R | \mathbf{H}_{z/n}))}_{\mathcal{L}_{\mathbf{y}_R}} \right. \\ &\quad + \underbrace{D_{\text{KL}}(q(\mathbf{z}_{t_m} | \mathbf{y}_R, \mathbf{z}_0, \mathbf{H}_{z/n}) \| p_{\theta}(\mathbf{z}_{t_m} | \mathbf{y}_R, \mathbf{H}_{z/n}))}_{\mathcal{L}_{t_m}} \\ &\quad + \sum_{n=2}^m \underbrace{D_{\text{KL}}(q(\mathbf{z}_{t_{n-1}} | \mathbf{z}_{t_n}, \mathbf{z}_0, \mathbf{H}_{z/n}) \| p_{\theta}(\mathbf{z}_{t_{n-1}} | \mathbf{z}_{t_n}, \mathbf{H}_{z/n}))}_{\mathcal{L}_{t_{n-1}}} \\ &\quad \left. - \underbrace{\log p_{\theta}(\mathbf{z}_{t_0} | \mathbf{z}_{t_1}, \mathbf{H}_{z/n})}_{\mathcal{L}_{t_0}} \right], \quad (28) \end{aligned}$$

where  $t_m$  is determined by  $\arg \min_{t_m} |\sigma^2 - t_m^2|$  and  $m$  denotes the utilized denoising steps of LDM with respect to terms  $\mathcal{L}_{\mathbf{y}_R}$  and  $\mathcal{L}_{t_m}$ . Evidently, assume that  $N > m$ , the terms  $\mathcal{L}_{t_{n-1}}$  and  $\mathcal{L}_{t_0}$  for wireless channel denoising are the sub-terms of the complete LDM training objectives. In other words, the selection of hyperparameters  $T$  or  $N$  should consider the possible worst SNRs of wireless channels. Ultimately, the transmitted latent vector  $\mathbf{z}_R$  is given by  $\mathbf{H}_z^{-1} \mathbf{z}_0$ . Nonetheless, in the wireless communication scenarios with low SNRs,  $m \gg 1$ . As a result, LDM will execute  $m$  times of noise predictions  $\epsilon_{\theta}(\mathbf{z}_t, t)$ , i.e., the number of function evaluation (NFE) reaches  $m$ . Unfortunately, the varying fading wireless channels with uncertain SNRs bring significant uncertainties to the computational complexity of LDM, which undermines the possibility of implementing real-time wireless SemCom.

### C. End-to-End Consistency Distillation

The multi-step reverse sampling process of DMs brings the disadvantage of slow data generation speed. To overcome it,



**Algorithm 4:** Sampling of channel denoising EECD

---

**Input:** Transmitted data  $\mathbf{x}$ , robust encoder  $E_{\phi'}(\cdot)$ , generator  $G_{\psi}(\cdot)$ , distilled end-to-end consistency model  $\mathbf{f}_{\theta}(\cdot, \cdot)$ , subsequence length  $s$ , and channel state information  $\mathbf{H}_z, \mathbf{H}_n, \sigma$

**Output:** Reconstructed data  $\hat{\mathbf{x}}$  at the receiver

- 1 Compute the encoded latent space  $\mathbf{z} \leftarrow E_{\phi'}(\mathbf{x})$ ;
- 2 Transmit real-valued  $\mathbf{z}_R$  through noisy wireless channel;
- 3 Compute MMSE equalization  $\mathbf{y}_R \leftarrow \mathbf{H}_z \mathbf{z}_R + \mathbf{H}_n \sigma \mathbf{\epsilon}$  and  $\mathbf{\epsilon} \sim \mathcal{N}(\mathbf{0}, \mathbf{I})$ ;
- 4 Estimate  $t_m$  by  $\arg \min_{t_m} |t_m^2 - \sigma^2|$ ;
- 5 Compute denoised estimation  $\hat{\mathbf{z}}_e \leftarrow \mathbf{f}_{\theta}(\mathbf{y}_R, t_m)$ ;
- 6 **if**  $s > 1$  **then**
- 7     Determine subsequence  $\tau = [\tau_1, \tau_2, \dots, \tau_s]$ ;
- 8     **for**  $i = 2$  **to**  $s$  **do**
- 9         Sample  $\mathbf{z}_{t_{\tau_i}} \sim \mathcal{N}(\mathbf{z}_{t_{\tau_i}}, \hat{\mathbf{z}}_e, t_{\tau_i}^2 \mathbf{H}_n^2 \mathbf{I})$ ;
- 10         Compute  $\hat{\mathbf{z}}_e \leftarrow \mathbf{f}_{\theta}(\mathbf{z}_{t_{\tau_i}}, t_{\tau_i})$ ;
- 11     **end**
- 12 **end**
- 13 Compute denoised data  $\hat{\mathbf{z}}_R \leftarrow \mathbf{H}_z^{-1} \hat{\mathbf{z}}_e$  and decoded  $\hat{\mathbf{z}}$ ;
- 14 **Return** the recovered data  $\hat{\mathbf{x}} \leftarrow G_{\psi}(\hat{\mathbf{z}})$

---

model can flexibly enhance the perceptual quality of reconstruction by resampling  $s - 1$  times based on the subsequence  $\tau = [\tau_1, \tau_2, \dots, \tau_s]$  of length  $s$ , where  $\tau_1 = m$ . Consequently, the real-time channel denoising and data reconstruction process based on EECD model is given in Algorithm 4. The advantages of utilizing the enhanced loss term to distill LDM are further elaborated as follows

- The training of the original LDM cannot optimize the generation of latent space together with the decoder  $G_{\psi}(\cdot)$ . However, the proposed end-to-end consistency loss allows the training objective to no longer be limited to mapping noisy equalization  $\mathbf{y}_R$  to the denoised latent space  $\hat{\mathbf{z}}_0$ , but directly measures the distance between reconstructed data of adjacent data points on the same trajectory.
- The latent consistency model cannot directly utilize more superior semantic metric functions such as LPIPS, while the EECD based loss effectively eliminates the limitation of only being able to calculate the distance between two latent bottlenecks.

## V. NUMERICAL EXPERIMENTS

### A. Experimental Setup

1) *Dataset:* MNIST handwritten digit image dataset is initially considered for evaluating the proposed SemCom system, containing 70,000 grayscale images of handwritten digits from 0 to 9, with 60,000 images for training and 10,000 for testing. Additionally, to validate the performance of out-of-distribution adaptation, the Fashion-MNIST (F-MNIST) dataset is also employed in the evaluation, comprising images of various types of clothing and accessories, with an identical distribution of 60,000 training and 10,000 testing images. The resolution for both MNIST and F-MNIST datasets are uniformly resized to 32×32. Furthermore, the animal face high quality (AFHQ) dataset [65] is also selected to verify the effectiveness, including a total of 15,000 RGB images across three categories: dogs, cats, and wild animals, where 4,500 images of dogs are used for training and the remaining 500 dog images, along

with 500 cat images, are used to test the proposed method, with the resolution resized to 192×192. Lastly, the DIV2K high-quality RGB image dataset [66] is also considered for SemCom tasks, encompassing 800 diverse training images, 100 validation images, and 100 test images, with the resolution resized to 256×256.

2) *Baseline Method:* Three distinct implementations of communication systems are utilized for comparison to demonstrate the superiority of the proposed SemCom system in terms of semantic reconstruction performance and real-time processing capabilities. The first is a combination of the state-of-the-art traditional image compression method JPEG2000 [10] with the error correction technique low-density parity check (LDPC) [67], denoted as JPEG2000+LDPC, which is a common method for image transmission in practical image communications. The second is the widely recognized VAE-based JSCC method [6], where joint source-channel training effectively mitigates the adverse effects of unreliable channels. The final approach is the multi-step VE-based LDM (VE-LDM) [40], which also serves as the teacher model for subsequent knowledge distillation.

3) *Performance Metrics:* The metrics for model evaluation can broadly be categorized into two types. The first category encompasses traditional bit/symbol accuracy metrics, including measures such as mean squared error (MSE) and peak SNR (PSNR). The second category consists of semantic or human-perceptual metrics that warrant increased attention within the context of SemCom, which for the transmission of images includes the multi-scale structural similarity index measure (MS-SSIM) [15] and the pretrained VGG-based LPIPS [64].

4) *CSI Condition:* For the wireless channels, three distinct channels are taken into consideration, including the AWGN channel ( $K = \infty$ ), the Rayleigh channel ( $K = 0$ ), and the Rician channel ( $K = 1$ ). Regarding the noise level of the channels, noise with SNRs ranging from 0dB to 20dB is contemplated for testing the performance of various methods under different SNR conditions. Lastly, for the channel bandwidth ratio (CBR), CBRs from 0.01 to 0.05 are implemented on DL models trained by AFHQ and DIV2K datasets, while for the MNIST dataset, only CBRs of 1/16 and 1/3 have been realized.

5) *Simulation Environment and Hyperparameters:* The simulations are conducted using Python 3.8.19 and CUDA-accelerated PyTorch 2.3.0 on a computer equipped with an i5-13600KF CPU operating at 3.50GHz, 32 GB of RAM, and an NVIDIA GeForce RTX 4070 GPU. Unlike the data generation task, the training for the wireless channel denoising task can follow a shorter time schedule. Consequently, the total length of the forward process for the LDM is set to  $N = 100$ , with the variance starting point at  $t_1 = \varepsilon = 0.002$  and the endpoint at  $t_N = T = 2$ , and  $\rho = 7.0$ . It is noteworthy that the image data has been transformed into values ranging from -1 to 1 with both variance and mean of 0.5, while the latent vector comprises data with a mean of 0 and a variance of 1. Furthermore, the learning rate during training is established at 1e-4, with an initial decay rate of 0.95 and a decay rate of 0.99993 for the student model.

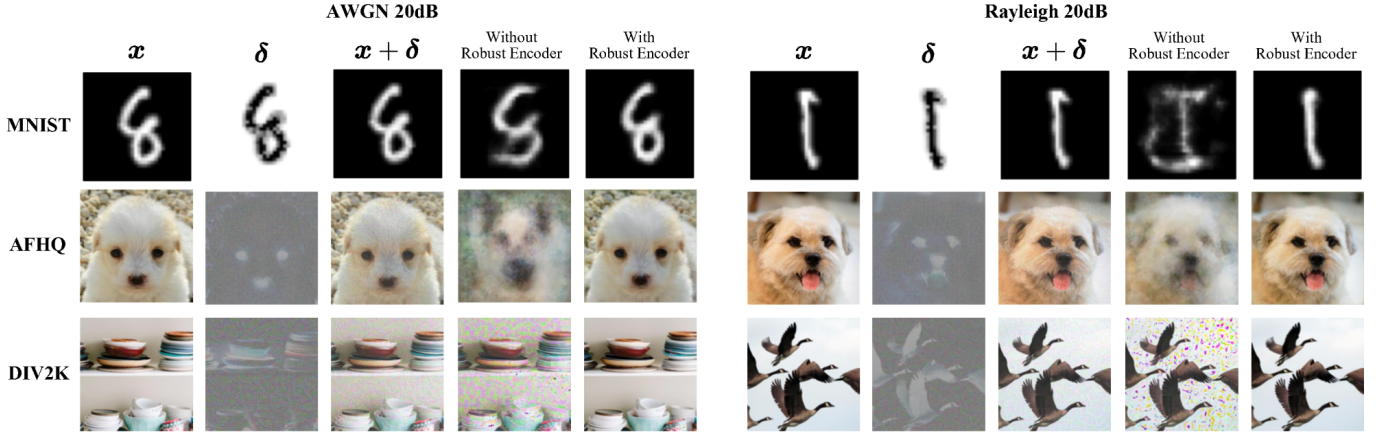


Fig. 5. Some typical decoded images without/with robust encoder in AWGN 20dB channel and Rayleigh 20dB channel.

### B. Robustness to Data Inaccuracies

As stated in Section III-C, The encoder parameters can be updated via augmented learning based on the obtained semantic errors  $\delta$ , ultimately endowing the DL-based SemCom system with robustness against various types of outliers. For the MNIST, AFHQ, and DIV2K datasets, encoders pretrained are updated with a learning process at an error level of  $\|\delta\|_p/H = 0.3$ , where  $H$  denotes the image resolution. Following the update, several prototypical image datasets are employed to test the robust encoder's efficacy in effectively countering data inaccuracies. Fig. 5 illustrates the impact of semantic errors with levels of 0.5 and 0.4 superimposed on the original data under AWGN 20dB and Rayleigh 20dB channel conditions, respectively. It is readily observed that the source data with added semantic errors still bear minimal semantic differences from the original data to the human visual perception. However, when the original SemCom system, without a robust encoder, transmits this contaminated data, the decoded output can result in significant semantic errors, such as the images of dog faces under AWGN 20dB channel conditions and handwritten digits and dog faces under Rayleigh 20dB channel conditions, and might also lead to extensive artifacts in reconstructed images as seen in the DIV2K dataset. Fortunately, the introduction of the robust encoder successfully overcomes semantic ambiguities that may arise from semantic errors or other types of outliers, ensuring that the decoded data at the receiver still carries the correct semantic information.

To maintain generality, the results of multiple performance tests for various outlier types and levels across different datasets are documented in Table I. Specifically, the CBR is fixed at approximately 0.02 and the test CSI conditions vary in accordance with Section V-A. It is not difficult to observe that the robust encoder, despite only being augmentedly trained at a semantic error level of 0.3, also maintains robustness compared to the original encoder under other semantic error levels and low-SNR noise contamination, thereby enhancing the quality of decoded data when source data is subjected to semantic errors or noises. Furthermore, evaluation metrics such as PSNR/SSIM/MS-SSIM can be improved by several times or even an order of magnitude, while MSE/LPIPS can be reduced by several times or even by an order of magnitude.

### C. Out-of-Distribution Adaptation

As described in Section III-D, the proposed SemCom system employs a lightweight, single-layer adapter at the transmitter for rapid one-shot learning and transforms the latent space at the receiver, thereby enabling the DL-based SemCom system to adapt to out-of-distribution data or enhance decoding quality. Specifically, subsets of clothing images from the F-MNIST dataset and cat images from the AFHQ dataset were utilized to validate the efficacy of the adapter. As illustrated in Fig. 6 and Fig. 7, without the adapter enabled, a SemCom system pretrained with a particular type of data would decode data at the receiver that more closely resembles that specific type of semantic information, leading to severe semantic ambiguity. However, the adapter situated before the generator can swiftly overcome this bottleneck, producing data that is essentially consistent with the original semantics of the transmitted data. Additionally, the original training DL model underperformed on certain test data from the DIV2K dataset, with decoded data exhibiting partial errors. The adapter also enhances communication quality in such instances, eliminating artifacts in the images.

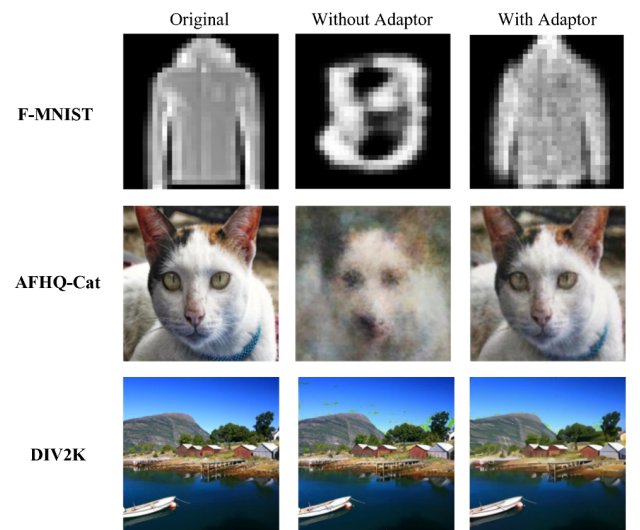


Fig. 6. Some typical decoded images without/with adaptor in AWGN 20dB channel.

TABLE I  
ROBUSTNESS OF SEMANTIC COMMUNICATION SYSTEM UNDER DIFFERENT LEVELS OF SEMANTIC ERRORS AND GAUSSIAN NOISES (WITHOUT ROBUST ENCODER/WITH ROBUST ENCODER), WHERE CBR IS FIXED AT 0.0208 AND CSI IS VARYING

Error/Noise Metric		$\ \delta\ _p / H$					SNR (dB)			
Error/Noise Level		0.1	0.2	0.3	0.4	0.5	5	7.5	10	12.5
MNIST	PSNR (dB)	16.54/18.50	11.88/18.52	8.33/18.60	5.96/16.36	5.16/12.42	6.17/8.16	7.52/11.35	10.05/14.91	12.30/17.10
	SSIM (dB)	10.65/13.32	5.72/13.56	2.77/13.19	1.18/10.56	0.76/6.79	1.40/3.52	2.21/5.15	4.01/8.60	5.77/11.18
	MSE	0.022/0.014	0.065/0.014	0.147/0.013	0.253/0.023	0.304/0.057	0.241/0.153	0.177/0.073	0.099/0.032	0.059/0.019
AFHQ	PSNR (dB)	22.31/22.51	18.94/22.14	15.34/21.58	12.82/21.38	9.72/20.58	13.56/15.24	18.45/19.19	21.20/21.89	22.32/21.19
	MS-SSIM (dB)	19.82/20.68	13.75/20.65	9.34/20.28	6.56/19.11	3.81/17.76	6.76/9.86	13.42/14.27	17.92/18.44	20.27/20.40
	LPIPS	0.160/0.152	0.211/0.157	0.302/0.158	0.410/0.172	0.531/0.180	0.475/0.348	0.246/0.226	0.175/0.172	0.154/0.151
DIV2K	PSNR (dB)	23.60/23.71	18.62/23.17	14.55/22.70	10.37/22.01	8.99/21.65	11.87/14.27	16.54/18.66	20.87/21.24	22.20/22.41
	MS-SSIM (dB)	16.19/16.49	10.20/16.28	8.22/16.01	6.01/15.88	4.94/15.19	5.66/8.39	11.09/12.73	13.68/15.11	15.35/16.22
	LPIPS	0.122/0.121	0.208/0.129	0.325/0.133	0.442/0.147	0.560/0.157	0.512/0.297	0.261/0.237	0.184/0.160	0.131/0.128

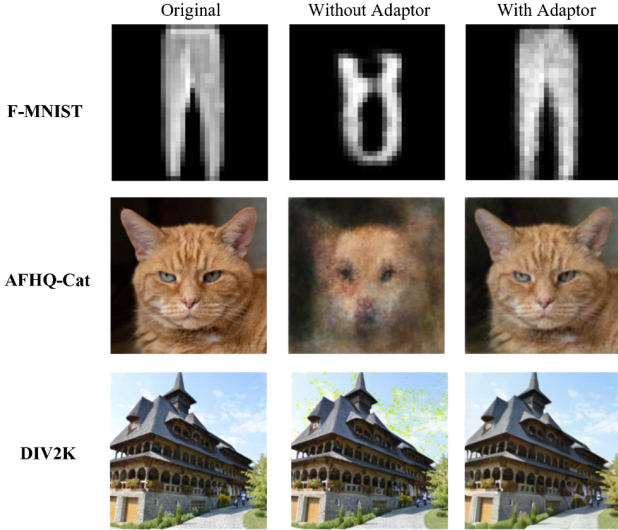


Fig. 7. Some typical decoded images without/with adaptor in Rayleigh 20dB channel.

The evolution of performance metrics during the one-shot learning process for the three datasets is depicted in Fig. 8. Evidently, after approximately only 20 epochs, the metrics of decoded data with adapters can be swiftly ameliorated to ideal values, thereby diminishing semantic ambiguities. To ensure generality, numerical experiments are also conducted to corroborate the effectiveness of the proposed adaptive strategy in enhancing SemCom performance and mitigating semantic ambiguity, with the results presented in Table II. Notably, as evidenced by the semantic evaluation metrics SSIM/MS-SSIM and LPIPS, the incorporation of adapters substantially augments the receiver's out-of-distribution adaptation and reconstruction capabilities under certain constraints on image categories, preventing the emergence of semantic ambiguities.

#### D. Channel Denoising Performance

The presence of varying fading gains and noise with uncertain SNRs in wireless channels can severely impair the efficacy of SemCom systems. Accordingly, denoising the noisy signals subsequent to equalization at the receiver emerges as a vital approach to safeguard the desired meaning of the transmitted

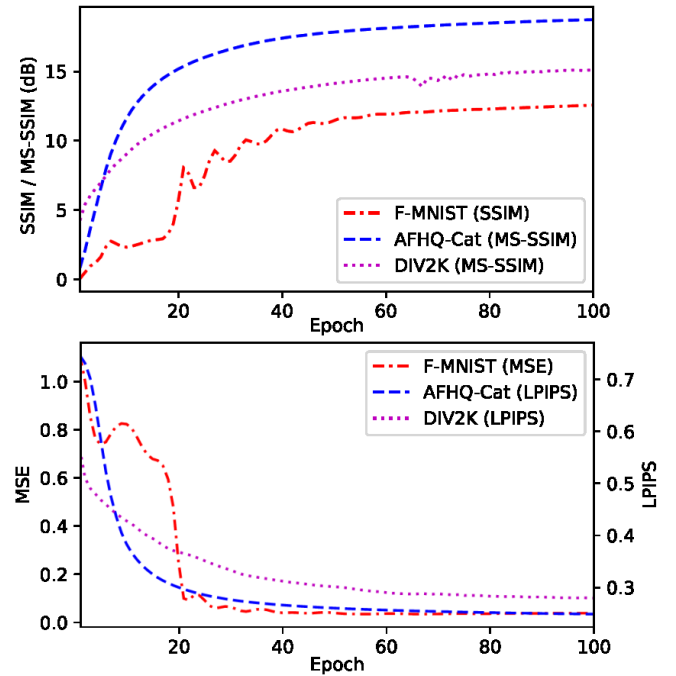


Fig. 8. The performance metrics' curves when do one-shot learning.

TABLE II  
IMPROVEMENT IN ADAPTION AND RECONSTRUCTION PERFORMANCE FOR DIFFERENT TYPES OF DATA (WITHOUT ADAPTOR/WITH ADAPTOR)

Dataset \ Metrics	PSNR (dB)	SSIM/MS-SSIM (dB)	MSE/LPIPS
F-MNIST	6.16/13.82	0.48/8.90	0.313/0.049
AFHQ-Cat	9.93/19.56	3.09/16.59	0.655/0.232
DIV2K	17.63/28.67	10.51/16.30	0.288/0.175

data. Typically, the channel denoising results of Deep JSCC, JPEG2000+LDPC, VE-LDM, and the proposed EECD methods are demonstrated in Fig. 9 under the conditions of both AWGN 10dB and Rayleigh 10dB. Herein, the conventional JPEG2000+LPDC approach configures CBR at 1/3 for MNIST and 0.05 for AFHQ/DIV2K datasets, whereas the CBR for DL-based methods is set at 1/16 for MNIST, and approximately

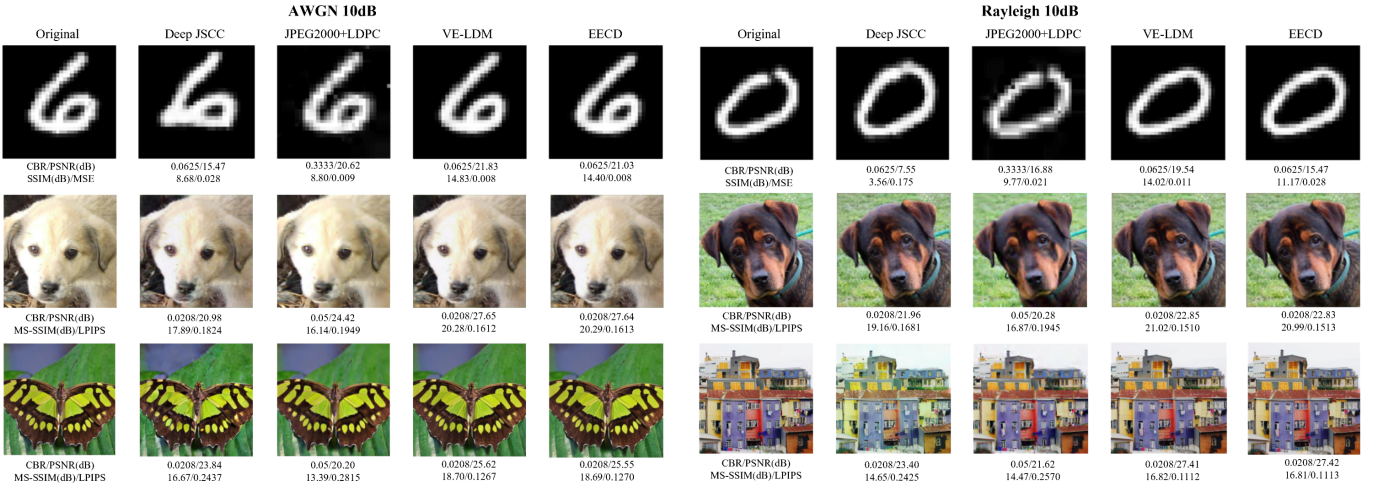


Fig. 9. Some typical decoded images with received latent space signals denoised by different approaches in AWGN 10dB channel and Rayleigh 10dB channel.

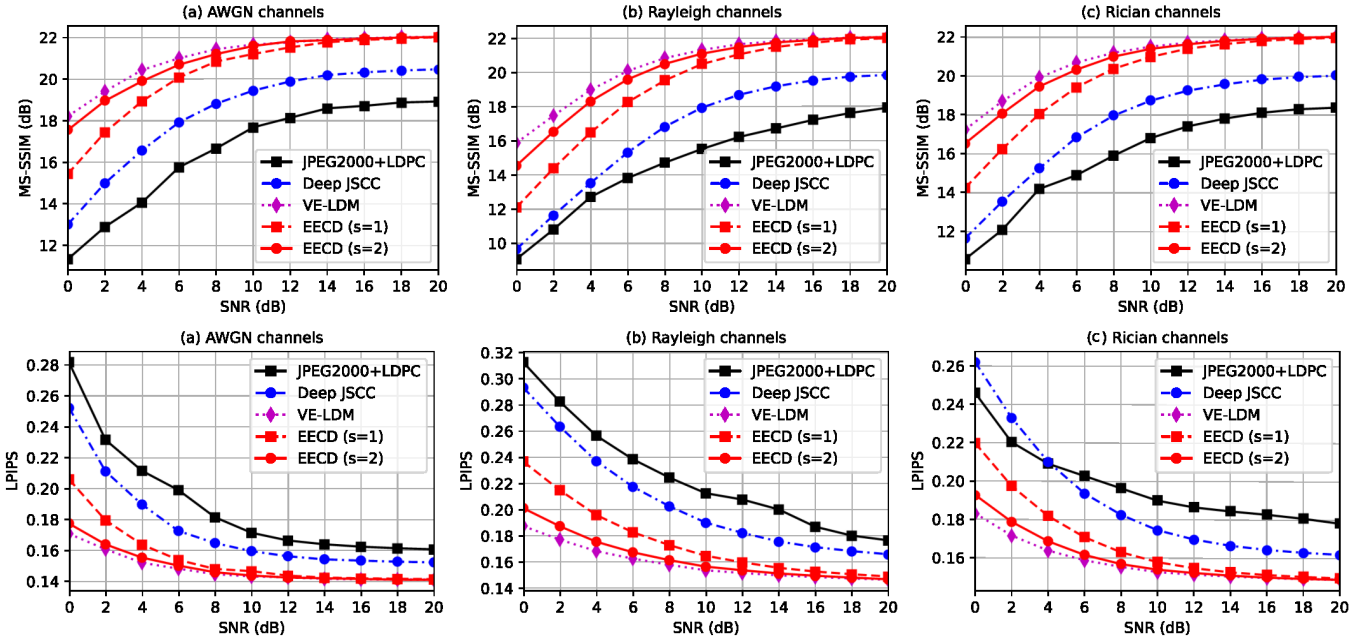


Fig. 10. Semantic metrics (MS-SSIM and LPIPS) of JPEG2000+LDPC, Deep JSCC, VE-LDM, and EECD methods under different SNRs and channel states within AFHQ dataset.

0.02 for AFHQ/DIV2K. It is noted that JPEG2000+LDPC suffers from partial bit errors and image blurring at a noise level of 10dB SNR, resulting in a lower MS-SSIM and a higher LPIPS than DL-based methods.

Advancing further into DL-based methods, SemCom systems constructed on DMs and GANs outperform those based on a VAE-based Deep JSCC approach. As depicted in Fig. 9, the Deep JSCC method exhibits a slight deficiency in certain image details relative to the latter two methods, leading to marginally inferior semantic metrics. Most crucially, the EECD method, with a subsequence length of  $s=2$  used for comparison, demonstrates that the EECD methodology based on VE-LDM distillation virtually matches the performance of the original teacher model under 10dB SNR noise levels, unequivocally attesting to the effectiveness and superiority of the proposed end-to-end human perception metric-based distillation strategy.

Numerical experiments conducted on the AFHQ dataset have provided ample validation for four distinct methodologies, revealing variations in two pivotal semantic metrics under various channel conditions and noise levels. Specifically, the CBR for JPEG2000+LDPC is set at 0.05, while a unified CBR of 0.02 is employed for the other DL-based methods. Notably, the EECD method employs different subsequence lengths of  $s=2$  and  $s=1$  to validate its denoising proficiency. As illustrated in Fig. 10, a perceptible degradation in quality is observed for all methods in the low-SNR area, with a particularly pronounced decline under Rayleigh and Rician channels, likely induced by fading gains. Conventionally, joint compression and error correction methods exhibit slightly inferior performance compared to DL-based approaches across varying SNRs and channel types. Furthermore, the VAE-based Deep JSCC method converges to a different perceptual quality level when compared to methods utilizing DMs and generator

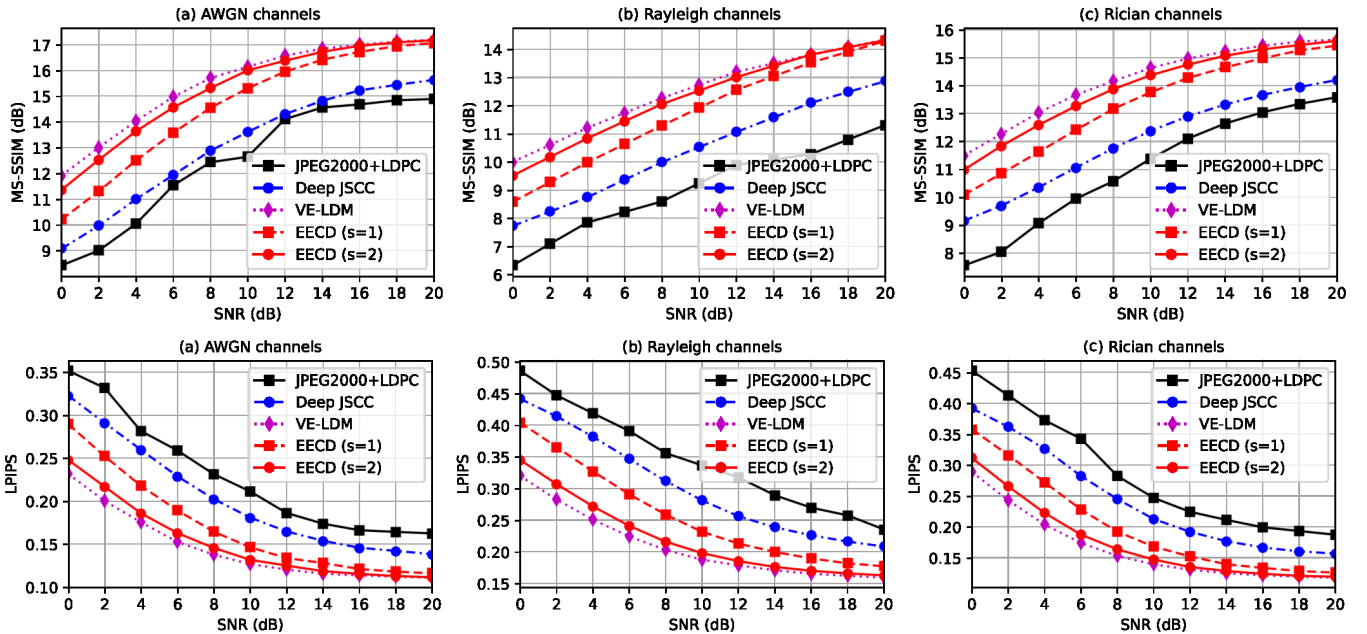


Fig. 11. Semantic metrics (MS-SSIM and LPIPS) of JPEG2000+LDPC, Deep JSCC, VE-LDM, and EECD methods under different SNRs and channel states within DIV2K dataset.

as SNR gradually increases. In contrast, VE-LDM and EECD methods converge to the same level of perceptual quality in high-SNR area. Most importantly, the performance of EECD can be further approximated to that of the teacher model, VE-LDM, with increased resampling length, even in low-SNR area.

Analogously, numerical experiments have been conducted within the DIV2K dataset, the results of which are depicted in Fig. 11. The CBR and CSI settings for four methods are consistent with those utilized in the numerical experiments for the AFHQ dataset. Specifically, the human-perceptual metrics for the denoising outcomes in the AWGN channel are superior to those in the Rayleigh and Rician channels. With regard to different channel denoising approaches, the original channel denoising DM undoubtedly achieved the most favorable performance, closely followed by the EECD curves with two different subsequence lengths, where the outcomes with  $s=2$  were highly proximate to the denoising effects of the original VE-LDM, ensuring the normal transmission of semantic information.

CBR is also an exceedingly crucial metric in SemCom, representing the ratio of transmitted bits/symbols to the size of the source data, and defining the demand for communication resources. Generally, an exemplary SemCom system is expected to maintain good reconstruction perceptual quality at a lower CBR, ultimately conserving communication bandwidth and reducing the communication burden. Fig. 12 presents the changes in average perceptual metrics for four different methods within the AFHQ dataset at CBRs ranging from 0.01 to 0.05. On one hand, the decoding quality of the conventional JPEG2000+LDPC method is heavily influenced by the compression ratio, with different CBRs potentially resulting in a manifold change in perceptual metrics. On the other hand, DL-based methods are less affected by CBR, indicating that DL-

based models are robust and excel at extracting data features in the low-CBR area. Moreover, the channel denoising methods constructed based on DMs have attained optimal performance under various CBR conditions.

#### E. Computational Complexity Analysis

Another paramount requirement for SemCom systems is low-latency communication, encompassing minimal data processing time for encoding, transmission, denoising, and decoding. This aspect significantly impacts the age of information (AoI), quality of service (QoS), and quality of experience (QoE). The introduction of the EECD method enables the distillation of the multi-step denoising process in the latent space of the original diffusion model into a few, or even a one-step sampling process, with only a slight perceptual quality trade-off, thus facilitating real-time SemCom. Specifically, since the VE-LDM and EECD methods both utilize the same robust encoder and generator, only the computational complexity of the denoising process is analyzed. As discussed in [42], the noise prediction time complexity for the denoising U-Net used by the diffusion model is

$$\text{Time} \sim \mathcal{O} \left( \sum_{l=1}^L h_l^2 w_l^2 \cdot C_l \cdot C_{l-1} \cdot K_l^2 \right), \quad (35)$$

where  $L$  is the number of layers,  $h_l w_l$  denotes the feature size and  $h_l w_l \propto H^2$ ,  $C_l$  and  $C_{l-1}$  are the number of convolutional kernels in the  $l$ -th and  $l-1$ -th layer, and  $K$  is the edge length of the convolutional kernel. The channel denoising task requires only  $m$  NFE based on the noise level, hence the sampling time complexity is  $\text{Time} \sim m \times \mathcal{O} \left( \sum_{l=1}^L h_l^2 w_l^2 \cdot C_l \cdot C_{l-1} \cdot K_l^2 \right)$ . Evidently, VE-LDM may not meet the real-time denoising requirements in scenarios with low-SNR, high-CBR, or high-resolution. As demonstrated by the time consumptions for different datasets under various CSI conditions in Table III, the

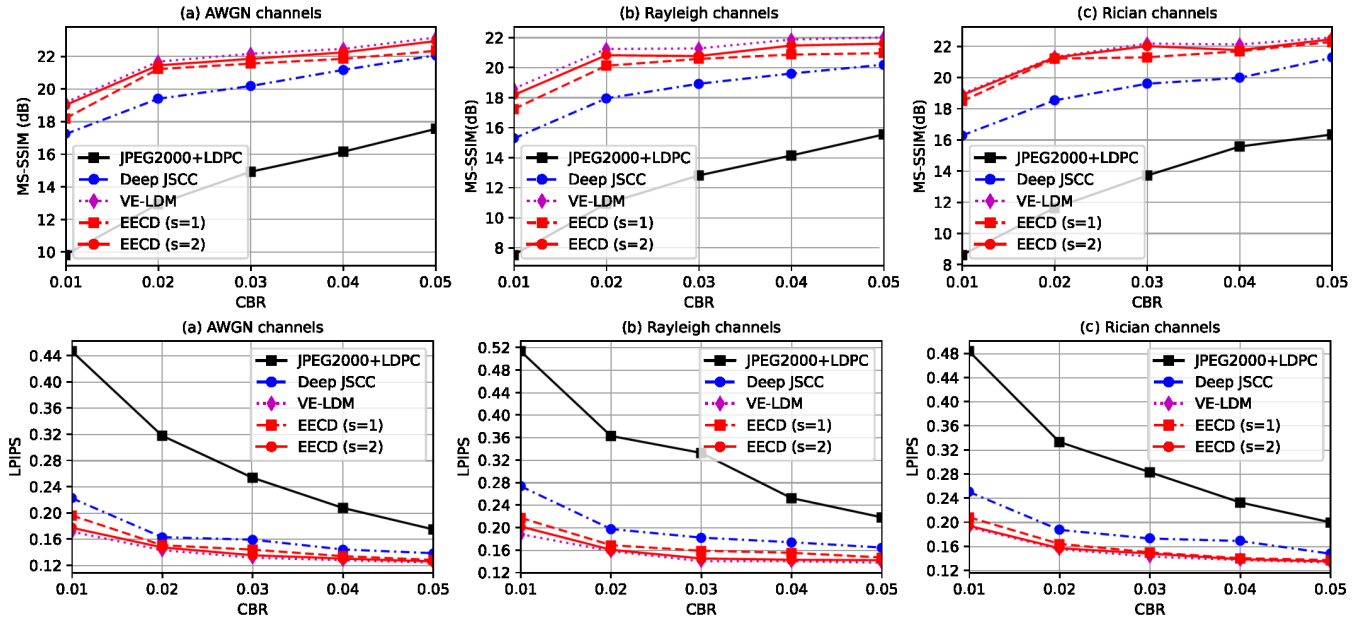


Fig. 12. Semantic metrics (MS-SSIM and LPIPS) of JPEG2000+LDPC, Deep JSCC, VE-LDM, and EECD methods under different CBRs within AFHQ dataset.

computing time of VE-LDM may vary dramatically according to the noise level. However, after the application of EECD, where the denoising steps are fixed at the setting value ( $s=2$ ), the overall time required for the encoding, denoising, and decoding sequence is substantially reduced to mere tens of milliseconds.

TABLE III

TIME CONSUMPTION FOR CHANNEL DENOISING UNDER DIFFERENT CSIs USING THE VARIANCE-EXPLODING BASED LATENT DIFFUSION MODEL AND THE PROPOSED EECD METHOD (VE-LDM/EECD (MILISECONDS))

CSI	SNR (dB)	MNIST	AFHQ	DIV2K
AWGN	0	762.3/32.7	749.6/36.4	832.6/43.0
	10	543.5/33.0	513.6/36.3	591.3/43.2
	20	361.7/32.9	326.4/36.6	396.7/43.1
Rayleigh	0	762.7/32.5	750.1/36.5	833.1/43.1
	10	543.7/33.2	514.1/36.3	590.9/43.0
	20	362.3/33.0	327.8/36.8	397.1/43.3
Rician	0	761.9/32.5	749.7/36.4	832.8/43.2
	10	542.9/32.9	513.7/36.4	591.4/43.3
	20	362.1/32.4	327.0/36.5	396.9/43.1

Within the AFHQ dataset, the time consumption variability of VE-LDM and EECD models trained at different CBRs across a SNR range from 0dB to 20dB is illustrated in Fig. 13. In conjunction with the data presented in Table III and Fig. 13, it is evident that both the CBR and the image resolution can influence the channel denoising processing time. However, the predominant factor affecting the VE-LDM during the denoising process is the noise level. Consequently, in contrast to the VE-LDM's more substantial and variable time complexity during denoising, the proposed EECD method consistently maintains the time required for single image transmission task within the scale of tens of milliseconds. Additionally, in line with the numerical results previously discussed, EECD does

not significantly degrade semantic quality across various CSI scenarios.

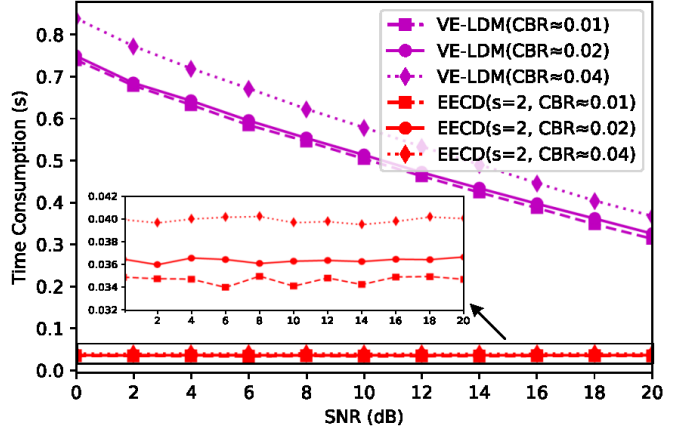


Fig. 13. Time consumptions of single image's encoding, denoising, and decoding process when utilizing VE-LDM and EECD methods under different CBRs and CSIs.

## VI. CONCLUSION

This paper introduces a wireless semantic communication (SemCom) system tailored to navigate the challenges of semantic ambiguities and channel noises. The proposed SemCom system's proficiency in feature extraction diminishes the adverse effects of outliers in source data on deep learning-based communication systems and exhibits an impressive aptitude for rapid adaptation to out-of-distribution data, thereby augmenting the human-perceptual quality of decoded data. In the realm of data transmission, the advanced end-to-end consistency distillation (EECD) strategy facilitates real-time channel denoising across various pre-estimated channel state information (CSI) scenarios, achieving this with minimal perceptual quality degradation when contrasted with

the existing channel denoising diffusion model techniques. Nonetheless, the real-time SemCom system based on diffusion models with unknown CSI and images with ultra-high resolution (2K/4K/6K) still warrants further investigation. Additionally, the integration of diffusion models into subsequent-generation communication paradigms, specifically goal/task-oriented SemCom systems, poses an intriguing and significant topic for future exploration.

## APPENDIX

### A. Variational Upper Bound Transformation

Proof of Eq. (4):

$$\begin{aligned}
 & \mathbb{E}_{q_\phi(z|x)} [-\log p_\psi(x|z)] + \mathbb{E}_{q_\phi(z|x)} [\log q_\phi(z|x)] \\
 &= \mathbb{E}_{q_\phi(z|x)} [-\log p_\psi(x|z)] + \mathbb{E}_{q_\phi(z|x)} \left[ \log \frac{q_\phi(z|x)}{p_\psi(z)} \right] \\
 &\quad \underbrace{\mathbb{E}_q [\mathcal{D}_{KL}(q_\phi(z|x) \| p_\psi(z))]} \\
 &\quad + \mathbb{E}_{q_\phi(z|x)} [\log p_\psi(z)] \\
 &\geq \mathbb{E}_{q_\phi(z|x)} \left[ \log \frac{q_\phi(z|x)}{p_\psi(z)} - \log p_\psi(x|z) \right] \\
 &= \int q_\phi(z|x) \log \frac{q_\phi(z|x)}{p_\psi(z|x)p_\psi(z)} dz \\
 &= \int q_\phi(z|x) \left[ \log p_\psi(x) + \log \frac{q_\phi(z|x)}{p_\psi(z|x)} \right] dz - \mathbb{E}_q [\log p_\psi(x)] \\
 &= \int q_\phi(z|x) \left[ \log \frac{q_\phi(z|x)}{p_\psi(z|x)} \right] dz + \mathbb{E}_q [-\log p_\psi(x)] \\
 &= \mathbb{E}_{q(x)} [\mathcal{D}_{KL}(q_\phi(z|x) \| p_\psi(z|x))] + \mathbb{E}_{q_\psi(z)} [-\log p_\psi(x)]. \tag{36}
 \end{aligned}$$

### B. Training Process of VAE-WGAN-GP

The training process is illustrated in Algorithm 5.

## REFERENCES

---

**Algorithm 5:** Training algorithm of VAE-WGAN-GP

---

**Input:** Dataset  $q(\mathbf{x})$ , learning rate  $\eta$ , gradient penalty coefficient  $\lambda$ , loss balance hyperparameters  $\alpha_\phi$  and  $\alpha_\psi$ , the number of iterations  $n_{critic}$  of discriminator per generator iteration, initial encoder parameter  $\phi$ , generator parameter  $\psi$ , discriminator parameter  $\gamma$

**Output:** The trained  $E_\phi(\cdot)$ ,  $G_\psi(\cdot)$ , and  $D_\gamma(\cdot)$

```

1 repeat
2   for  $i = 0, \dots, n_{critic}$  do
3     Sample  $\mathbf{x} \sim q(\mathbf{x})$ ,  $\mathbf{z} \sim q_\psi(\mathbf{z})$ , and  $\epsilon_1, \epsilon_2 \sim U[0, 1]$ ;
4     Compute  $\hat{\mathbf{x}}_1 \leftarrow \epsilon_1 \mathbf{x} + (1 - \epsilon_1) G_\psi(\mathbf{z})$ ;
5     Compute  $\hat{\mathbf{x}}_2 \leftarrow \epsilon_2 \mathbf{x} + (1 - \epsilon_2) G_\psi(E_\phi(\mathbf{x}))$ ;
6     Update  $\gamma$  by
7        $\gamma \leftarrow \gamma - \eta \nabla_\gamma \left[ \mathbb{E}_q \left( -2D_{\gamma(\mathbf{x})} + D_\gamma(G_\psi(\mathbf{z})) + D_\gamma(G_\psi(E_\phi(\mathbf{x}))) + \lambda (\|\nabla_{\hat{\mathbf{x}}_1} D_\gamma(\hat{\mathbf{x}}_1)\|_2 - 1)^2 + \lambda (\|\nabla_{\hat{\mathbf{x}}_2} D_\gamma(\hat{\mathbf{x}}_2)\|_2 - 1)^2 \right) \right]$ ;
8   end
9   Sample  $\mathbf{x} \sim q(\mathbf{x})$  and  $\mathbf{z} \sim q_\psi(\mathbf{z})$ ;
10  Update  $\phi$  by
11     $\phi \leftarrow \phi - \eta \nabla_\phi \left[ \mathbb{E}_q \left( \alpha_\phi \mathcal{D}_{KL}(E_\phi(\mathbf{x}) \sim \mathcal{N}(\mu, \sigma^2) \| \mathbf{z} \sim \mathcal{N}(\mathbf{0}, \mathbf{I})) + (1 - \alpha_\phi) \mathcal{D}_{KL}(G_\psi(E_\phi(\mathbf{x})) \| \mathbf{x}) \right) \right]$ ;
12  Update  $\psi$  by
13     $\psi \leftarrow \psi - \eta \nabla_\psi \left[ \mathbb{E}_q \left( \alpha_\phi \mathcal{D}_{KL}(G_\psi(E_\phi(\mathbf{x})) \| \mathbf{x}) + (1 - \alpha_\phi) (-D_\gamma(G_\psi(\mathbf{z})) - D_\gamma(G_\psi(E_\phi(\mathbf{x})))) \right) \right]$ ;
11 until Converged;
12 Return Trained VAE-WGAN-GP Model

```

---

[1] Y. Siriwardhana, P. Porambage, M. Liyanage, and M. Ylianttila, “A survey on mobile augmented reality with 5g mobile edge computing: Architectures, applications, and technical aspects,” *IEEE Communications Surveys & Tutorials*, vol. 23, no. 2, pp. 1160–1192, 2021.

[2] X. Huang, J. Riddell, and R. Xiao, “Virtual reality telepresence: 360-degree video streaming with edge-compute assisted static foveated compression,” *IEEE Transactions on Visualization and Computer Graphics*, 2023.

[3] F. E. Abrahamsen, Y. Ai, and M. Cheffena, “Communication technologies for smart grid: A comprehensive survey,” *Sensors*, vol. 21, no. 23, p. 8087, 2021.

[4] W. Wu, F. Zhou, B. Wang, Q. Wu, C. Dong, and R. Q. Hu, “Unmanned aerial vehicle swarm-enabled edge computing: Potentials, promising technologies, and challenges,” *IEEE Wireless Communications*, vol. 29, no. 4, pp. 78–85, 2022.

[5] M. Z. Chowdhury, M. Shahjalal, S. Ahmed, and Y. M. Jang, “6g wireless communication systems: Applications, requirements, technologies, challenges, and research directions,” *IEEE Open Journal of the Communications Society*, vol. 1, pp. 957–975, 2020.

[6] E. Bourtsoulatz, D. Burth Kurka, and D. Gündüz, “Deep joint source-channel coding for wireless image transmission,” *IEEE Transactions on Cognitive Communications and Networking*, vol. 5, no. 3, pp. 567–579, 2019.

[7] J. Xu, T.-Y. Tung, B. Ai, W. Chen, Y. Sun, and D. D. Gündüz, “Deep joint source-channel coding for semantic communications,” *IEEE Communications Magazine*, vol. 61, no. 11, pp. 42–48, 2023.

[8] G. Ginesu, M. Pintus, and D. D. Giusto, “Objective assessment of the webp image coding algorithm,” *Signal processing: image communication*, vol. 27, no. 8, pp. 867–874, 2012.

[9] G. K. Wallace, “The jpeg still picture compression standard,” *IEEE transactions on consumer electronics*, vol. 38, no. 1, pp. xviii–xxxiv, 1992.

[10] C. Christopoulos, A. Skodras, and T. Ebrahimi, “The jpeg2000 still image coding system: an overview,” *IEEE transactions on consumer electronics*, vol. 46, no. 4, pp. 1103–1127, 2000.

[11] Y. Fan, J. Yu, and T. S. Huang, “Wide-activated deep residual networks based restoration for bpg-compressed images,” in *Proceedings of the IEEE conference on computer vision and pattern recognition Workshops*, 2018, pp. 2621–2624.

[12] W. Yang *et al.*, “Semantic communications for future internet: Fundamentals, applications, and challenges,” *IEEE Communications Surveys & Tutorials*, vol. 25, no. 1, pp. 213–250, 2022.

[13] X. Luo, H.-H. Chen, and Q. Guo, “Semantic communications: Overview, open issues, and future research directions,” *IEEE Wireless Communications*, vol. 29, no. 1, pp. 210–219, 2022.

[14] H. Xie, Z. Qin, G. Y. Li, and B.-H. Juang, “Deep learning enabled semantic communication systems,” *IEEE Transactions on Signal Processing*, vol. 69, pp. 2663–2675, 2021.

[15] J. Dai *et al.*, “Nonlinear transform source-channel coding for semantic communications,” *IEEE Journal on Selected Areas in Communications*, vol. 40, no. 8, pp. 2300–2316, 2022.

[16] K. He, X. Zhang, S. Ren, and J. Sun, “Deep residual learning for image recognition,” in *Proceedings of the IEEE conference on computer vision and pattern recognition*, 2016, pp. 770–778.

[17] J. Xu, B. Ai, W. Chen, A. Yang, P. Sun, and M. Rodrigues, “Wireless image transmission using deep source channel coding with attention modules,” *IEEE Transactions on Circuits and Systems for Video Technology*, vol. 32, no. 4, pp. 2315–2328, 2021.

[18] N. Farsad, M. Rao, and A. Goldsmith, “Deep learning for joint source-channel coding of text,” in *2018 IEEE international conference on acoustics, speech and signal processing (ICASSP)*. IEEE, 2018, pp. 2326–2330.

[19] H. Zhang, S. Shao, M. Tao, X. Bi, and K. B. Letaief, “Deep learning-enabled semantic communication systems with task-unaware transmitter and dynamic data,” *IEEE Journal on Selected Areas in Communications*, vol. 41, no. 1, pp. 170–185, 2022.

[20] D. Huang, F. Gao, X. Tao, Q. Du, and J. Lu, “Toward semantic communications: Deep learning-based image semantic coding,” *IEEE Journal on Selected Areas in Communications*, vol. 41, no. 1, pp. 55–71, 2022.

[21] Z. Weng and Z. Qin, “Semantic communication systems for speech transmission,” *IEEE Journal on Selected Areas in Communications*, vol. 39, no. 8, pp. 2434–2444, 2021.

[22] H. Xie, Z. Qin, X. Tao, and K. B. Letaief, “Task-oriented multi-user semantic communications,” *IEEE Journal on Selected Areas in Communications*, vol. 40, no. 9, pp. 2584–2597, 2022.

[23] J. Ho, A. Jain, and P. Abbeel, “Denoising diffusion probabilistic models,” *Advances in neural information processing systems*, vol. 33, pp. 6840–6851, 2020.

[24] J. Song, C. Meng, and S. Ermon, “Denoising diffusion implicit models,” *arXiv preprint arXiv:2010.02502*, 2020.

[25] D. P. Kingma and M. Welling, “Auto-encoding variational bayes,” *arXiv preprint arXiv:1312.6114*, 2013.

[26] I. Goodfellow *et al.*, “Generative adversarial networks,” *Communications of the ACM*, vol. 63, no. 11, pp. 139–144, 2020.

[27] G. Papamakarios, E. Nalisnick, D. J. Rezende, S. Mohamed, and B. Lakshminarayanan, “Normalizing flows for probabilistic modeling and inference,” *Journal of Machine Learning Research*, vol. 22, no. 57, pp. 1–64, 2021.

[28] H. Du *et al.*, “Beyond deep reinforcement learning: A tutorial on generative diffusion models in network optimization,” *arXiv preprint arXiv:2308.05384*, 2023.

[29] H. Du, J. Wang, D. Niyato, J. Kang, Z. Xiong, and D. I. Kim, “Ai-generated incentive mechanism and full-duplex semantic communications for information sharing,” *IEEE Journal on Selected Areas in Communications*, 2023.

[30] J. Chen, D. You, D. Gündüz, and P. L. Dragotti, “Commin: Semantic image communications as an inverse problem with inn-guided diffusion models,” in *ICASSP 2024-2024 IEEE International Conference on Acoustics, Speech and Signal Processing (ICASSP)*. IEEE, 2024, pp. 6675–6679.

[31] E. Grassucci, S. Barbarossa, and D. Comminiello, “Generative semantic communication: Diffusion models beyond bit recovery,” *arXiv preprint arXiv:2306.04321*, 2023.

[32] S. F. Yilmaz, X. Niu, B. Bai, W. Han, L. Deng, and D. Gunduz, “High perceptual quality wireless image delivery with denoising diffusion models,” *arXiv preprint arXiv:2309.15889*, 2023.

[33] M. Yang, D. Gao, F. Xie, J. Li, X. Song, and G. Shi, “Sg2sc: A generative semantic communication framework for scene understanding-oriented image transmission,” in *ICASSP 2024-2024 IEEE International Conference on Acoustics, Speech and Signal Processing (ICASSP)*. IEEE, 2024, pp. 13 486–13 490.

[34] Y. Choukroun and L. Wolf, “Denoising diffusion error correction codes,” *arXiv preprint arXiv:2209.13533*, 2022.

[35] N. Zilberstein, A. Swami, and S. Segarra, “Joint channel estimation and data detection in massive mimo systems based on diffusion models,” in *ICASSP 2024-2024 IEEE International Conference on Acoustics, Speech and Signal Processing (ICASSP)*. IEEE, 2024, pp. 13 291–13 295.

[36] F. Jiang *et al.*, “Large generative model assisted 3d semantic communication,” *arXiv preprint arXiv:2403.05783*, 2024.

[37] Z. Jiang, X. Liu, G. Yang, W. Li, A. Li, and G. Wang, “Diffsc: Semantic communication framework with enhanced denoising through diffusion probabilistic models,” in *ICASSP 2024-2024 IEEE International Conference on Acoustics, Speech and Signal Processing (ICASSP)*. IEEE, 2024, pp. 13 071–13 075.

[38] E. Grassucci, C. Marinoni, A. Rodriguez, and D. Comminiello, “Diffusion models for audio semantic communication,” in *ICASSP 2024-2024 IEEE International Conference on Acoustics, Speech and Signal Processing (ICASSP)*. IEEE, 2024, pp. 13 136–13 140.

[39] H. Du *et al.*, “Exploring collaborative distributed diffusion-based ai-generated content (aigc) in wireless networks,” *IEEE Network*, 2023.

[40] T. Wu *et al.*, “Cdmd: Channel denoising diffusion models for wireless semantic communications,” *IEEE Transactions on Wireless Communications*, pp. 1–1, 2024.

[41] M. Kim, R. Fritschek, and R. F. Schaefer, “Learning end-to-end channel coding with diffusion models,” in *WSA & SCC 2023; 26th International ITG Workshop on Smart Antennas and 13th Conference on Systems, Communications, and Coding*, 2023, pp. 1–13.

[42] J. Pei, J. Wang, D. Shi, and P. Wang, “Detection and imputation based two-stage denoising diffusion power system measurement recovery under cyber-physical uncertainties,” *IEEE Transactions on Smart Grid*, pp. 1–1, 2024.

[43] D. Adesina, C.-C. Hsieh, Y. E. Sagduyu, and L. Qian, “Adversarial machine learning in wireless communications using rf data: A review,” *IEEE Communications Surveys & Tutorials*, vol. 25, no. 1, pp. 77–100, 2022.

[44] G. Zhang, Q. Hu, Z. Qin, Y. Cai, and G. Yu, “A unified multi-task semantic communication system with domain adaptation,” in *GLOBECOM 2022-2022 IEEE Global Communications Conference*. IEEE, 2022, pp. 3971–3976.

[45] J. Adler and S. Lunz, “Banach wasserstein gan,” *Advances in neural information processing systems*, vol. 31, 2018.

[46] Y. Song, P. Dhariwal, M. Chen, and I. Sutskever, “Consistency models,” *arXiv preprint arXiv:2303.01469*, 2023.

[47] A. Vahdat, K. Kreis, and J. Kautz, “Score-based generative modeling in latent space,” *Advances in neural information processing systems*, vol. 34, pp. 11 287–11 302, 2021.

[48] R. Rombach, A. Blattmann, D. Lorenz, P. Esser, and B. Ommer, “High-resolution image synthesis with latent diffusion models,” in *Proceedings of the IEEE/CVF conference on computer vision and pattern recognition*, 2022, pp. 10 684–10 695.

[49] G. Zheng *et al.*, “Mobility-aware split-federated with transfer learning for vehicular semantic communication networks,” *IEEE Internet of Things Journal*, pp. 1–1, 2024.

[50] R. Abdal, Y. Qin, and P. Wonka, “Image2stylegan: How to embed images into the stylegan latent space?” in *Proceedings of the IEEE/CVF international conference on computer vision*, 2019, pp. 4432–4441.

[51] Z. Wang, H. Zheng, P. He, W. Chen, and M. Zhou, “Diffusion-gan: Training gans with diffusion,” *arXiv preprint arXiv:2206.02262*, 2022.

[52] W. Luo, T. Hu, S. Zhang, J. Sun, Z. Li, and Z. Zhang, “Diff-instruct: A universal approach for transferring knowledge from pre-trained diffusion models,” *Advances in Neural Information Processing Systems*, vol. 36, 2024.

[53] W. Xia, Y. Zhang, Y. Yang, J.-H. Xue, B. Zhou, and M.-H. Yang, “Gan inversion: A survey,” *IEEE transactions on pattern analysis and machine intelligence*, vol. 45, no. 3, pp. 3121–3138, 2022.

[54] I. Gulrajani, F. Ahmed, M. Arjovsky, V. Dumoulin, and A. C. Courville, “Improved training of wasserstein gans,” *Advances in neural information processing systems*, vol. 30, 2017.

[55] R. B. Lanfredi, J. D. Schroeder, and T. Tasdizen, “Quantifying the preferential direction of the model gradient in adversarial training with projected gradient descent,” *Pattern Recognition*, vol. 139, p. 109430, 2023.

[56] T. Cemgil, S. Ghaisas, K. D. Dvijotham, and P. Kohli, “Adversarially robust representations with smooth encoders,” in *International Conference on Learning Representations*, 2019.

[57] D. Pasquini, M. Mingione, and M. Bernaschi, “Adversarial out-domain examples for generative models,” in *2019 IEEE European Symposium on Security and Privacy Workshops (EuroS&PW)*. IEEE, 2019, pp. 272–280.

[58] T. Karras, M. Aittala, T. Aila, and S. Laine, “Elucidating the design space of diffusion-based generative models,” *Advances in Neural Information Processing Systems*, vol. 35, pp. 26 565–26 577, 2022.

[59] F. Bao, C. Li, J. Sun, J. Zhu, and B. Zhang, “Estimating the optimal covariance with imperfect mean in diffusion probabilistic models,” *arXiv preprint arXiv:2206.07309*, 2022.

[60] S. Luo, Y. Tan, L. Huang, J. Li, and H. Zhao, “Latent consistency models: Synthesizing high-resolution images with few-step inference,” *arXiv preprint arXiv:2310.04378*, 2023.

[61] C. Lu, Y. Zhou, F. Bao, J. Chen, C. Li, and J. Zhu, “Dpm-solver++: Fast solver for guided sampling of diffusion probabilistic models,” *arXiv preprint arXiv:2211.01095*, 2022.

[62] Z. Zhou, D. Chen, C. Wang, and C. Chen, “Fast ode-based sampling for diffusion models in around 5 steps,” *arXiv preprint arXiv:2312.00094*, 2023.

[63] T. Huang *et al.*, “Knowledge diffusion for distillation,” *Advances in Neural Information Processing Systems*, vol. 36, 2024.

[64] R. Zhang, P. Isola, A. A. Efros, E. Shechtman, and O. Wang, “The unreasonable effectiveness of deep features as a perceptual metric,” in *Proceedings of the IEEE conference on computer vision and pattern recognition*, 2018, pp. 586–595.

[65] Y. Choi, Y. Uh, J. Yoo, and J.-W. Ha, “Stargan v2: Diverse image synthesis for multiple domains,” in *Proceedings of the IEEE/CVF conference on computer vision and pattern recognition*, 2020, pp. 8188–8197.

[66] R. Timofte *et al.*, “Ntire 2018 challenge on single image super-resolution: Methods and results,” in *The IEEE Conference on Computer Vision and Pattern Recognition (CVPR) Workshops*, June 2018.

[67] J. Chen, A. Dholakia, E. Eleftheriou, M. P. Fossorier, and X.-Y. Hu, “Reduced-complexity decoding of ldpc codes,” *IEEE transactions on communications*, vol. 53, no. 8, pp. 1288–1299, 2005.